



What is the real role of iron oxides in the optical properties of dust aerosols?

X. L. Zhang^{1,2}, G. J. Wu², C. L. Zhang³, T. L. Xu^{2,4}, and Q. Q. Zhou¹

¹Key laboratory of Wetland Ecology and Environment, Northeast Institute of Geography and Agroecology, Chinese Academy of Sciences, Changchun 130102, China

²Key Laboratory of Tibetan Environment Changes and Land Surface Processes, Institute of Tibetan Plateau Research, CAS Center for Excellence and Innovation in Tibetan Plateau Earth System Sciences, Chinese Academy of Sciences, Beijing 100101, China

³Research Center for Eco-Environmental Sciences, Chinese Academy of Sciences, Beijing 100085, China

⁴University of Chinese Academy of Sciences, Beijing 100049, China

Correspondence to: X. L. Zhang (zhangxuelei@neigae.ac.cn) and G. J. Wu (wugj@itpcas.ac.cn)

Received: 16 January 2015 – Published in Atmos. Chem. Phys. Discuss.: 26 February 2015

Revised: 26 September 2015 – Accepted: 15 October 2015 – Published: 3 November 2015

Abstract. Iron oxide compounds constitute an important component of mineral dust aerosols. Several previous studies have shown that these minerals are strong absorbers at visible wavelengths and thus that they play a critical role in the overall climate perturbation caused by dust aerosols. When compiling a database of complex refractive indices of possible mineral species of iron oxides to study their optical properties, we found that uniformly continuous optical constants for a single type of iron oxide in the wavelength range between 0.2 and 50 μm are very scarce, and that the use of hematite to represent all molecular or mineral iron-oxides types is a popular hypothesis. However, the crucial problem is that three continuous data sets for complex refractive indices of hematite are employed in climate models, but there are significant differences between them. Thus, the real role of iron oxides in the optical properties of dust aerosols becomes a key scientific question, and we address this problem by considering different refractive indices, size distributions and more logical weight fractions and mixing states of hematite. Based on the microscopic observations, a semi-external mixture that employs an external mixture between Fe aggregates and other minerals and partly internal mixing between iron oxides and aluminosilicate particles is advised as the optimal approximation. The simulations demonstrate that hematite with a spectral refractive index from Longtin et al. (1988) shows approximately equal absorbing capacity to the mineral illite over the whole wavelength region

from 0.55 to 2.5 μm , and only enhances the optical absorption of aerosol mixture at $\lambda < 0.55 \mu\text{m}$. Using the data set from Querry (1985) may overestimate the optical absorption of hematite at both visible and near-infrared wavelengths. More laboratory measurements of the refractive index of iron oxides, especially for hematite and goethite in the visible spectrum, should therefore be taken into account when assessing the effect of mineral dust on climate forcing.

1 Introduction

Iron oxides in dusts are now identified as being an important component for a number of climatic, environmental and biological processes. Over the past decade, iron-oxide minerals have been shown to be able to strongly absorb solar radiation (Tegen et al., 1997; Sokolik and Toon, 1999; Lafon et al., 2004; Qin and Mitchell, 2009; Redmond et al., 2010), and thus have a direct impact on the Earth's radiation balance (Balkanski et al., 2007; Smith and Grainger, 2014; Scanza et al., 2015). Based on the ability to absorb acidic gases and water vapour (Baltrusaitis et al., 2007; Wijenayaka et al., 2012; Song and Boily, 2013), iron oxides also contribute to heterogeneous reactions and cloud processes (Shi et al., 2011; Dupart et al., 2012), further influencing the radiation balance. In particular, layers of dust on snow and ice cover accelerate the melting of snow and ice by diminishing

the surface albedo (Painter et al., 2010; Ginot et al., 2014), and the heat-absorbing properties of iron oxides in these dust layers can add to this effect (Kaspari et al., 2014; Reynolds et al., 2013; Dang and Hegg, 2014). Moreover, the deposited iron-bearing dust aerosols provide critical nutrients to marine and terrestrial ecosystems, which are associated with consequential important drawdown of atmospheric carbon dioxide (Jickells et al., 2005; Shao et al., 2011; Nickovic et al., 2013). However, these effects can lead to either positive or negative net radiative forcing, depending mostly on the underlying surface albedo, vertical profile (optical depth and height of dust layer), particle size distribution and mineralogy (Liao and Seinfeld, 1998; Claquin et al., 1999). This large uncertainty results from our limited knowledge of the physical, chemical and optical properties of atmospheric iron oxides on various space and timescales (Tegen et al., 1997; Sokolik et al., 2001; Formenti et al., 2011).

The element iron can be found among numerous mineralogical species, such as feldspars, clays (e.g. illite, smectite, chlorite and biotite), iron oxides or iron hydroxides. A useful mineralogical classification frequently used in soil science distinguishes two categories of iron: (i) “structural iron” (in either the Fe(II) or Fe(III) oxidation states), trapped in the crystal lattice of aluminosilicate minerals; and (ii) iron (in the Fe(III) oxidation state), in the form of discrete oxide or hydroxide particles (Lafon et al., 2004). According to the classical terminology of soil scientists (Sumner, 1963; Anderson and Jenne, 1970; Angel and Vincent, 1978), the latter kind of iron will be referred to as free iron and its corresponding oxides and hydroxides as iron oxides. Indeed, 10 of 16 known iron oxides, hydroxides and oxide hydroxides are known to occur in nature, with goethite, hematite and magnetite being the most abundant as rock-forming minerals; ferrihydrite, maghemite and lepidocrocite being intermediately abundant in many locations; and wüstite, akaganéite, ferroxhyte and bernalite being the least abundant (Cornell and Schwertmann, 2006; Guo and Barnard, 2013). Dust aerosols from arid and semi-arid regions typically contain goethite, hematite, ferrihydrite and magnetite, and based on the mass contribution, hematite and goethite are the major components of free iron in atmospheric dust aerosols (Schroth et al., 2009; Shi et al., 2012; Takahashi et al., 2013). Hematite (Fe₂O₃) is very common in hot, dry soils and imparts a red colour to its sediments. Goethite (α -FeOOH) is a common weathered product in soils and loesses. It occurs in moist, acidic soils (Schwertmann, 1993) and is brown to yellow in colour.

Sokolik and Toon (1999) found that hematite is an especially strong absorber at ultraviolet (UV) and visible wavelengths, and it can also enhance the absorption of clay minerals and quartz through the formation of aggregates. Derimian et al. (2008) mentioned that iron oxides (primarily hematite and goethite) only affect the optical-absorbing ability of aeolian dust at short wavelengths (the blue spectral region). Since the importance of hematite relative to other dust mineral components was discussed more fully in the study of

Sokolik and Toon (1999), most subsequent modelling studies have assumed the iron oxides in dust aerosols to be in the form of hematite. An opposite viewpoint was put forward, however, by Balkanski et al. (2007), who have argued that the optical absorption of dust with hematite at visible wavelengths might be lower than previously thought. The main reason is that internal mixing rule calculations with a hematite content of 1.5 volume % (or 2.8 weight %) were supposed to be representative for median dust absorption and were, as well, consistent with the AERONET measurements.

However, recent measurements on dust samples from east Asia, northern Africa and western Africa (Lafon et al., 2006; Formenti et al., 2008; Reynolds et al., 2014) indicated that goethite was presented in higher concentration than hematite (i.e. the ratio of goethite to hematite is about 7 : 3, a result that will be detail introduced in Sect. 3.2.2). For dust in snow, goethite is also the dominant ferric oxide that is detected by reflectance spectroscopy, and thus appears to be the main iron-oxide control on absorption of solar radiation (Reynolds et al., 2013). More recently hematite and goethite have been taken into account interactively in global climate simulations due to the availability of global mineralogical distribution maps (Nickovic et al., 2012; Journet et al., 2014).

Furthermore, Müller et al. (2009) have measured the spectral imaginary refractive indices of hematite over the wavelengths from 590 to 790 nm during laboratory experiments, but these derived values are much lower than the data employed in Sokolik and Toon (1999). The theoretical simulations of optical scattering of hematite and goethite at 470, 550 and 660 nm by Meland et al. (2011) also found that differences are apparent for hematite in both the phase function and polarization results at 660 nm, where the imaginary indices from different references differ. Additionally, two studies that refer to optical properties of hematite in dust samples have also argued that the imaginary values of the hematite refractive index in Sokolik and Toon (1999) are more than a factor of 2 larger than those reported by Bedidi and Cervelle (1993) and Longtin et al. (1988) at wavelengths below 600 nm (Moosmüller et al., 2012; Wagner et al., 2012).

Thus, what is the real role of iron oxides in determining the overall impact of the optical properties of dust aerosols? This study will focus on investigating this important scientific question by considering heterogeneous optical refractive indices, mixing states and more logical abundance of iron oxides.

2 Method and simulation

2.1 Complex refractive index

The complex refractive index (optical constant) is the most basic and significant parameter for calculating the optical properties of aerosols, but values for the optical constants of hematite in the wavelength range 0.2 to 50 μ m are scarce

in published references. Table 1 compiles information about the complex refractive indices of the major constituents of free iron that we have found in the published literature. Sokolik and Toon (1999) employed the refractive indices of hematite from Querry et al. (1978), but the study by Querry et al. (1978) mainly considered the optical constants of limestone and, as far as we can discover, does not contain any work on hematite at all. Since the publication of Sokolik and Toon (1999), studies (Höller et al., 2003; Alfaro et al., 2004; Muñoz et al., 2006; Mishra and Tripathi, 2008; Otto et al., 2009; Meland et al., 2011; Wagner et al., 2012) have misquoted the data as Querry et al. (1978) or Querry (1987) when modelling the optical properties of hematite. Actually, Querry (1987) is entitled “Optical constants of minerals and other materials from the millimeter to the UV” and gives optical constants of 29 materials, but still without referring to hematite. After careful searching, we have found that Querry (1985) has tabulated values for the refractive index ($m = n + ki$) of hematite. Moreover, Longtin et al. (1988) also reported spectral refractive indices for hematite from earlier measurements by Steyer (1974), Onari et al. (1977), Galuza et al. (1979) and Kerker et al. (1979). This data set also has been used in modelling the contribution of hematite to the optical properties of atmospheric dust aerosols in recent studies (Klaver et al., 2011a; Köhler et al., 2011; Hansell Jr. et al., 2011). Recently, the third unpublished continuous refractive indices of hematite (named TA2005 in Table 1) from the Aerosol Refractive Index Archive (ARIA) of Oxford University have been employed in the Community Atmosphere Model (Scanza et al., 2015). Because this work has not been peer-reviewed and because TA2005 and QE1985 (see Table 1) show a similar wavelength dependency, we pay special attention to the differences of refractive indices between QE1985 and LG1988 in this paper. Any errors due to uncertainties in the optical constants would be directly reflected in the calculated results referred to above.

Bedidi and Cervelle (1993) also presented refractive indices for hematite and goethite derived from reflectance measurements at wavelengths of 350–750 nm. Glotch and Rogers (2007) reported the optical constants of hematite, goethite and magnetite over the infrared (IR) wavelengths, and Hsu and Matijević (1985) also measured the refractive indices of hematite in the wavelengths of 350–650 nm.

Hematite is a uniaxial crystal that crystallizes in the trigonal system, whose optic axis corresponds to the crystallographic c axis. Perpendicular to the c axis are two radial a axes. The dielectric constants of bulk hematite must therefore be measured for two principal polarizations of the incident light, namely, one with the electric vector in any direction perpendicular to the c axis (the so-called ordinary ray or – O-ray) and the other with the electric vector along the crystalline c axis (the extraordinary ray or – E-ray). In this work we have calculated the average refractive indices for anisotropic hematite from all references in Table 1. The for-

mula used is adopted from Longtin et al. (1988) and is

$$m_{\text{avg}} = (2n_{\text{E-ray}}/3 + n_{\text{O-ray}}/3) + (2k_{\text{E-ray}}/3 + k_{\text{O-ray}}/3)i. \quad (1)$$

The reported values for the complex refractive index from the sources in Table 1 are markedly different, especially the imaginary part that controls the optical absorption. In order to visually demonstrate the variation of optical constants from different references, values of the real (n) and logarithmic values of imaginary parts (k) are shown in Fig. 1.

For the real part of the refractive index for iron oxides, there is a reasonable agreement between the hematite and magnetite data sets from the different references (Fig. 1c). Because the real refractive index of hematite shows large fluctuations at wavelengths longer than 18 μm due to anisotropic refraction, the agreement between the different data sets decreases at these wavelengths. For goethite we are aware of only two sets of optical constants: one at visible wavelengths from Bedidi and Cervelle (1993) and the other at IR wavelengths from Glotch and Rogers (2007), but the wavelength gap between these two data sets hampers continuity. Unfortunately, Meland et al. (2011) have checked the former data set for goethite using simulations according to Mie and T-matrix theories and show that it may be in error. Nevertheless, we can see that goethite has optical constants similar to hematite. The real refractive index of hematite is larger than that of magnetite at wavelengths less than 2 μm , but is smaller between 2 and 33 μm (Fig. 1c and d).

For the imaginary part of the refractive index of iron oxides, hematite and goethite have different optical properties at short wavelengths, both in terms of magnitude and spectral dependence (Bedidi and Cervelle, 1993). Between 460 and 700 nm, the imaginary part of the complex refractive index (representing absorption) of goethite is up to 3 times smaller than that of hematite. As a consequence, the proportions of hematite and goethite in mineral dust can potentially change the magnitude and the spectral dependence of shortwave absorption of mineral dust. However, the limited and discontinuous refractive indices of goethite have constrained the evaluation of the effects of specific compositions of goethite and hematite to dust optical properties and solar radiation balance over broader wavelength ranges.

From Fig. 1a, we clearly see that the k values for hematite from QE1985 and from LG1988 show significant differences for wavelengths between 650 nm and 15 μm . These differences are present at visible wavelengths and disappear at ultraviolet wavelengths, but the two data sets have similar trends at UV and visible wavelengths (Fig. 1b). Note that the hematite optical constants vary dramatically across the visible wavelengths. In particular, the imaginary part of the index for hematite shows a sharp decrease with increasing wavelength in the red. As a consequence there is a large variability in the imaginary refractive index values for hematite taken from different published references, particularly at 2 μm where the values from different sources differ by a factor of 8600. Thus, this study firstly focuses on what will be

Table 1. Summary of the published complex refractive indices for major constituents of free iron at different wavelengths (with their references).

Iron-oxide species	Wavelength (μm)	Reference source	Abbreviation
Hematite	8.3–50	Popova et al. (1973)	PV1973
Hematite	1.0–333	Onari et al. (1977)	OA1977
Hematite	0.25–0.7	Shettle and Fenn (1979)	SF1979
Hematite	0.35–0.65	Hsu and Matijević (1985)	HM1985
Hematite	0.21–90	Querry (1985)	QE1985
Hematite	0.3–300	Longtin et al. (1988)	LG1988
Hematite	0.2–0.7	Gillespie and Lindberg (1992)	GL1992
Hematite	0.2–4.5	Krekov (1992)	KE1992
Hematite	0.35–0.75	Bedidi and Cerville (1993)	BC1993
Hematite	0.1–1000	Triaud (unpublished data)*	TA2005
Hematite	5–50	Marra et al. (2005)	MR2005
Hematite	5–2000	Glotch and Rossman (2009)	GR2009
Hematite	0.59–0.79	Müller et al. (2009)	ML2009
Magnetite	0.21–55	Querry (1985)	QE1985
Magnetite	5–50	Mukai (1989)	MK1989
Magnetite	0.25–0.7	Gillespie and Lindberg (1992)	GL1992
Magnetite	0.1–1000	Amaury et al. (unpublished data)*	AU2002
Magnetite	5–100	Glotch and Rossman (2009)	GR2009
Goethite	0.45–0.75	Bedidi and Cerville (1993)	BC1993
Goethite	8–50	Glotch and Roman (2009)	GR2009
Wüstite	0.2–500	Henning (1995)	HN1995
Wüstite	10–500	Henning and Mutschke (1997)	HN1997

* The data were taken from <http://www.atm.ox.ac.uk/project/RI/hematite.html> and <http://www.astro.uni-jena.de/Laboratory/OCDB/mgfeoxides.html>.

the result if these heterogeneous optical constants of hematite are used as input for the calculation of radiation transfer models.

2.2 Particle size distribution

Size distribution is another important factor that affects the optical properties of particles. Because Sokolik and Toon (1999) have employed the refractive index data set for hematite from QE1985 to calculate the radiative properties, we adopt here the same particle size distribution but with the refractive index data set for hematite from LG1988 to compare our results with Sokolik and Toon (1999). The lognormal number size distribution is applied to dust aerosols:

$$n_n(\ln r) \equiv \frac{dN}{d\ln r} = \frac{N_0}{\sqrt{2\pi} \ln \sigma} \exp \left[-\frac{1}{2} \left(\frac{\ln r - \ln r_0}{\ln \sigma} \right)^2 \right], \quad (2)$$

where r_0 is the median radius, σ is the geometric standard deviation and N_0 is the total particle number density of the component in particles per cubic centimetre.

In order to compare with the results of Sokolik and Toon (1999), the optical properties of minerals are calculated on the assumption that they have one size mode but varying median radii. The particle size modes are selected as $r_0 = 0.5$ and $0.7 \mu\text{m}$, and $\sigma = 2.0$. The size mode with a median radius of $r_0 = 0.5 \mu\text{m}$ is believed to be representative of the particle size distribution of the long-lived, long-distance-transport

mode of airborne dust (Patterson and Gillette, 1977; Arimoto et al., 1997). The larger r_0 is representative of a particle size mode that occurs near the dust source (Gomes and Gillette, 1993). In reality, the size distribution of dust aerosols can have one or several modes, characterized by a specific composition (Mahowald et al., 2013).

2.3 Theoretical simulations

Images from scanning electron microscopy (SEM) reveal non-spherical, irregular and compact shapes of the dust particles (Fig. 3), but Otto et al. (2009) and Klaver et al. (2011b) have shown that spherical/non-spherical differences only influence the single-scattering albedo by less than 1 %. Meland et al. (2011) have also shown that moderate departures from spherical shape are relatively unimportant in determining the scattering matrix for particles with high refractive index values, such as hematite. Therefore, we expect the aerosol asphericity to have a negligible impact on our calculated results of optical properties and subsequent calculations using the Mie theory (which assumes a spherical morphology for the dust particles).

There are several different computer codes that can be used to compute optical properties for a lognormal particle size distribution. The theoretical light scattering simulations in this paper have used the MieTab software. MieTab uses a FORTRAN code with continued fraction mod-

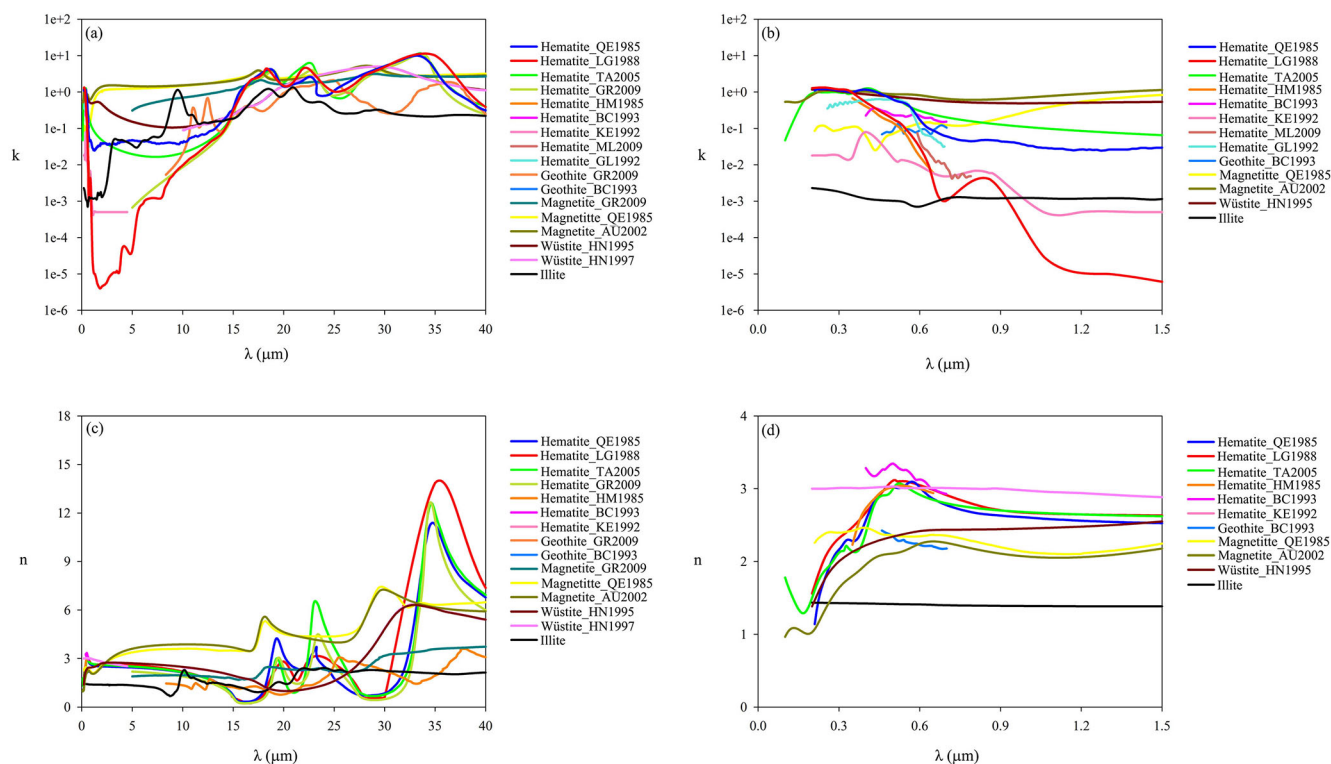


Figure 1. Spectral distribution of the imaginary and real parts of the complex refractive index for different iron oxides from Table 1 at wavelengths of 0 to 40 μm (a and c) and expanded for wavelengths of 0 to 1.5 μm (b and d).

ification produced by W. J. Lentz from the Mie code originally developed by Dave and Center (1968). This modified code can be obtained from <http://diogenes.iwt.uni-bremen.de/vt/laser/codes/ddave.zip>. In order to validate the accuracy of MieTab, we first compared it with a double precision Lorenz–Mie scattering code and a double precision T-matrix code for a lognormal particle size distribution from Mishchenko et al. (2002). The double precision Lorenz–Mie and T-matrix codes are available from http://www.giss.nasa.gov/staff/mmishchenko/t_matrix.html.

In addition to the wavelength-dependent optical constants and the size distribution, the T-matrix theory also requires assumptions about the particle shape. In this work we use an aspect ratio of 1.000001 to represent a spherical particle shape, because use of an aspect ratio exactly equal to 1 causes computational overflow in some cases. The calculated results from the three codes at different wavelengths and complex refractive indices for the same size distribution are listed in Table 2. The good agreement of the results from the three codes demonstrates that the possibility of computational error affecting the interpretation of the calculated optical properties of iron oxides can be neglected.

3 Results and discussion

3.1 Basic optical properties

We focus here on modelling the spectral optical properties of iron oxides that are needed for climate modelling: the volume extinction coefficient β_{ext} (which is the sum of the scattering coefficient β_{sca} and the absorption coefficient β_{abs}), the single-scattering albedo ω_0 and the asymmetry parameter g (a cosine weighted integral of the scattering phase function). This set of parameters allows for the calculation of radiation forcing in most climate models. Figure 2 shows calculated optical parameters for hematite (with complex refractive indices from QE1985 and LG1988) and illite with varying median radii at solar and infrared wavelengths. The volume total extinction coefficients β_{ext} have been normalized as β_{ext}^* for particle number concentration $N = 1 \text{ cm}^{-3}$.

Figure 2a and b demonstrate how the normalized spectral extinction coefficient and the normalized spectral absorption coefficient vary due to the differences in the refractive indices and median radii of the minerals. As shown in Fig. 2a, β_{ext}^* for hematite has a spectrum which is clearly distinguishable from that for illite at UV, visible and IR wavelengths. One point should be noted: hematite has a lower normalized spectral extinction coefficient than illite at wavelengths less than 1.3 μm , which means that hematite has a weaker optical extinction capacity than illite at these wavelengths. In the IR

Table 2. Comparison of simulated optical properties between MieTab, Lorenz–Mie and T-matrix methods.

Wavelength	550 nm			633 nm			1060 nm		
	$n = 3.102, k = 0.0925$			$n = 3.007, k = 0.00974$			$n = 2.66, k = 0.00003$		
$m = n+ki$ Code type	MieTab	T-matrix	Lorenz–Mie	MieTab	T-matrix	Lorenz–Mie	MieTab	T-matrix	Lorenz–Mie
Q_{ext}	2.0950	2.1332	2.1637	2.1440	2.1917	2.2585	2.3250	2.5042	2.0226
Q_{sca}	1.2640	1.3284	1.3233	1.8500	1.9048	1.9587	2.3240	2.5033	2.0216
Q_{abs}	0.8310	0.8048	0.8404	0.2940	0.2870	0.2998	0.0010	0.0009	0.0010
ω_0	0.6033	0.6227	0.6116	0.8629	0.8691	0.8673	0.9996	0.9996	0.9995

region, the spectral features of hematite in β_{ext}^* show large differences in volatility, and mimic the features in the refractive index of hematite. The magnitude of β_{ext}^* depends on the parameters of the particle size distribution.

Figure 2b shows the equivalent normalized spectral absorption coefficient for hematite from QE1985 and LG1988 at wavelengths less than 5 μm . The normalized absorption coefficient of hematite from QE1985 is about 100 times larger than that for illite at both visible and near-IR wavelengths, but the normalized absorption coefficient for hematite from LG1988 has larger values than those for illite at wavelengths less than 1 μm and values about 100 times smaller than those for illite at wavelengths between 1 and 5 μm . If we adopt the complex refractive indices of QE1985, the calculated absorption coefficient of hematite indicates that hematite is an especially strong absorber at UV and visible wavelengths. Conversely, the calculated absorption coefficient of hematite using LG1988 data suggests that hematite is an important aerosol component only for short-wavelength absorption. Considering the whole region from 0.2 to 5 μm , hematite with complex refractive indices from LG1988 has an approximately equal absorbing capacity to that of illite.

Figure 2c illustrates the single-scattering albedo of hematite and illite at wavelengths between 0.2 and 5 μm for different particle size distributions. The single-scattering albedo of hematite is about 0.6 for wavelengths $\lambda < 0.55 \mu\text{m}$ and varies little from $r_0 = 0.7 \mu\text{m}$ to $r_0 = 0.5 \mu\text{m}$. In contrast, illite has ω_0 in the range from about 0.9 to 1 for $\lambda < 0.55 \mu\text{m}$, showing strong spectral dependence at short wavelengths. For $\lambda > 0.55 \mu\text{m}$, illite has ω_0 of about 0.99 for $0.55 < \lambda < 2.0 \mu\text{m}$ and this gradually reduces to about 0.5 for $2.0 < \lambda < 5.0 \mu\text{m}$, while hematite shows large differences of ω_0 depending on the source of the refractive indices. The single-scattering albedo decreases to about 0.35 at UV wavelengths for hematite nanoparticles (which are always observed as aggregates with other clay mineral particles) with $r_0 = 0.01 \mu\text{m}$ and $\sigma = 2.0$, but it rapidly increases to nearly 1 at wavelengths $\lambda > 0.7 \mu\text{m}$.

Figure 2d compares the asymmetry parameter of hematite with refractive indices from QE1985 and LG1988 at UV and visible wavelengths with size modes of $r_0 = 0.7, 0.5$ and $0.01 \mu\text{m}$. For $r_0 = 0.5$ and $0.7 \mu\text{m}$, hematite from QE1985 has $g = 0.3\text{--}0.99$, g decreasing as λ increases. The magnitudes

of g from LG1988 are in the range from 0.2 to 0.99 with a few fluctuations. For $r_0 = 0.01 \mu\text{m}$, both data sets put g in the range from about 0.15 to 0.38. Thus, the magnitude of g depends significantly on the particle size distribution.

3.2 Physical and mineralogical properties

3.2.1 Size and morphology

Many electron microscopy observations (Greenland et al., 1968; Tipping, 1981; Postma and Brockenhuus-Schack, 1987; Poulton and Canfield, 2005; Raiswell and Anderson, 2005; Shi et al., 2009; Deboudt et al., 2012; Wagner et al., 2012; Guo and Barnard, 2013) have shown that poorly ordered iron oxides commonly occur as spheroidal to ellipsoidal nanoparticles that may be single or aggregated, and may be unattached or attached to quartz or clay minerals (Fig. 3). The reasons for the aggregation and the attachment are not well understood but are likely to be related to interactions of surface charge characteristics between iron oxides and quartz or clay minerals (Poulton and Canfield, 2005). According to Hinds (1982), the binding mechanisms that hold separate aerosols together in an agglomerate formed in the air include the van der Waals force, the electrostatic force and the surface tension of adsorbed liquid films. As mentioned above, the dispersed nanoparticles of iron oxides, which are attracted to larger dust particles, have more prominent optical absorption than aggregated iron oxides, but the use of size distributions for nanoparticles (such as $r_0 = 0.01 \mu\text{m}$ and $\sigma = 2.0$) will overestimate the optical absorption of iron oxides in natural dust aerosol samples.

3.2.2 Abundance of total iron and iron oxides

By employing the optical parameters of hematite and clay minerals calculated above, we can model the optical effects of hematite in dust aerosols. Problems associated with this are the actual variation of iron-oxide content and the state of the mixture with other minerals, and these should be accounted for when modelling the optical properties of dust aerosols.

The total iron content in dust aerosol bulk samples is always measured in terms of the Fe_2O_3 mass percentage of the total oxide mass by elemental analysis (i.e. XRF, PIXE or

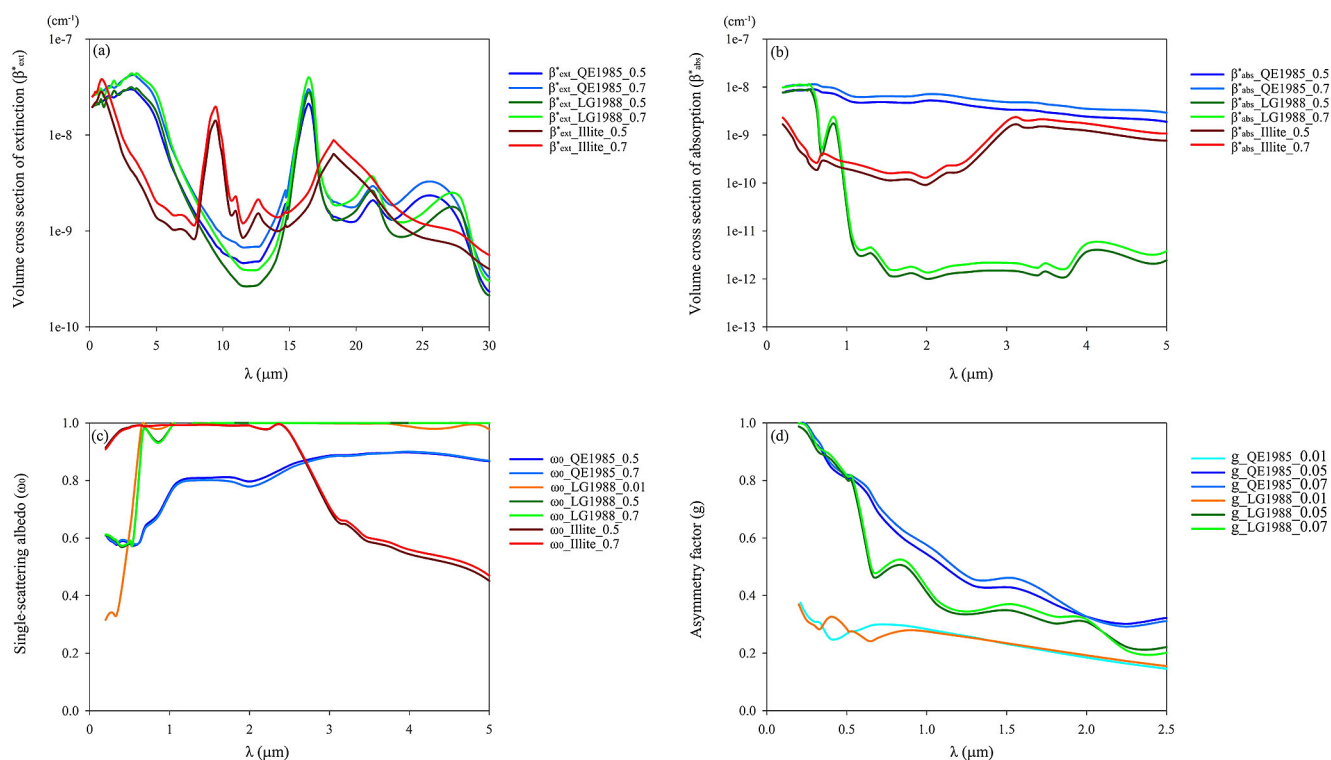


Figure 2. The calculated spectral optical properties for hematite, goethite and illite with different complex refractive index and size distribution. **(a)** Volume cross section of extinction, **(b)** volume cross section of absorption, **(c)** single-scattering albedo and **(d)** asymmetry factor.

ICP). Ganor and Foner (1996) gave a median Fe content of 2.9 % for dust storms in Israel. The observed Fe percentage for the Dunhuang site in China during the Asian Pacific Regional Aerosol Characterization Experiment (ACE-Asia) is 4.0 ± 0.9 % (Zhang et al., 2003). A value of 4.45 ± 0.49 % (Guieu et al., 2002) has been proposed as characterizing Saharan dust. The elemental analysis by X-ray fluorescence (XRF) yielded total iron oxides contents between 2.0 and 5.0 wt % for four Saharan mineral dust samples of different colour and origin (Linke et al., 2006). Moreover, Lafon et al. (2004, 2006) reported that the total iron content (the Fe_2O_3 percentage) varies from 6.2 to 8.7 % in six atmospheric samples and three wind tunnel generated samples. The total iron content ranges from 1.82 to 11.8 % (with an especially high value of 30.0 % in the sample collected from Bamako, Mali) in entrained $\text{PM}_{2.5}$ from 10 soil samples representing the Arabian Peninsula, the Sahara and Sahel regions and samples from northeast Africa and south-central Asia (Moosmüller et al., 2012). Furthermore, percentage values of iron content from several data sets reported by previous studies vary mainly between 4 and 11 % (e.g. Gomes and Gillette, 1993; Chiapello et al., 1997; Gao et al., 2001; Journet et al., 2014).

One additional aspect should be discussed here for the proper interpretation of the obtained data: how representative is the total iron concentration of the free iron oxide con-

tent of dust aerosols? Free iron is present as a major aerosol component affecting the short-wavelength absorption of mineral dust. However, iron oxide represents only part of the total iron, which may also exist in the crystal lattice of numerous other dust minerals. The iron oxide-to-total-iron ratio in natural and soil-derived aerosols has been characterized by applying an adapted reductive extraction method as commonly used in soil science (Lafon et al., 2004, 2006). This method provides no structural information about the extractable iron and therefore cannot distinguish between the presence of goethite or hematite in the samples. Fortunately this method can provide an upper limited to the free-iron content for the optical modelling.

Lafon et al. (2004, 2006) reported considerable variability in the iron oxide-to-total iron ratio for various regions and sampling conditions and that there is no clear relationship between the oxide-to-total iron ratio and dust origin or aging. Based on all the values for the oxide-to-total iron ratio reported in the published literature (Lafon et al., 2004, 2006; Alfaro et al., 2004; Formenti et al., 2008; Klaver et al., 2011a), we have calculated an average of 0.52. Formenti et al. (2014a) reported that iron oxides account, by mass, for 0.38 to 0.72 of the total elemental iron based on X-ray absorption analysis of samples of mineral dust emitted from or transported to western Africa. Reynolds et al. (2013) reported that the percent iron in goethite and hematite relative to iron

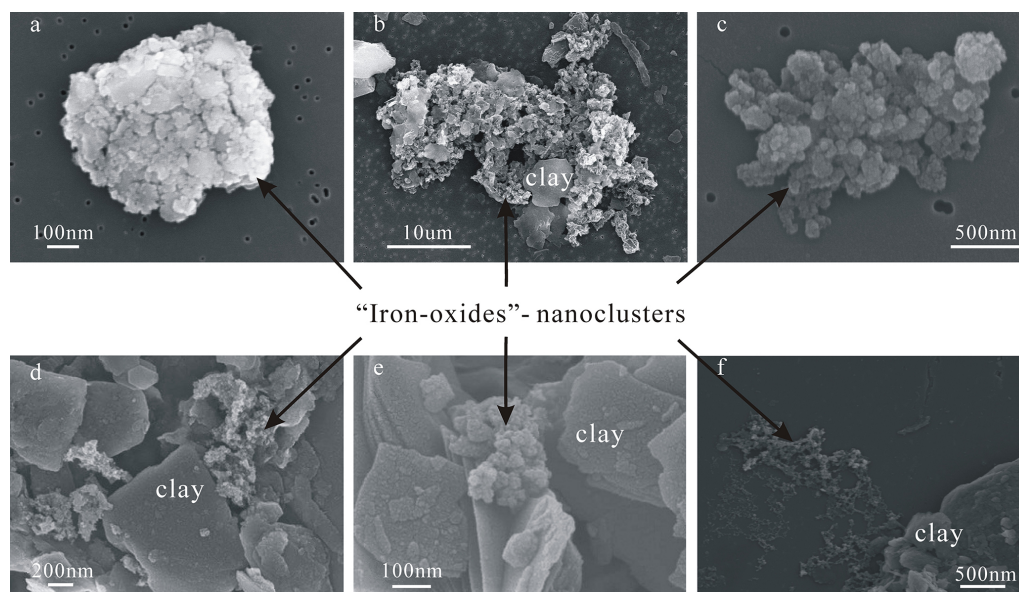


Figure 3. Representative morphology of iron-oxide aggregates in dust samples observed by SEM.

in all iron-bearing phases ranges from 0.2 to 0.52 for dust samples in Australia as determined from Mössbauer spectra. Based on an average compiled from the literature, Kandler et al. (2009) and Kandler et al. (2011) have assumed that only 20% of the total iron content is hematite when determining the complex refractive index of dust aerosols. Alfaro et al. (2004) found in their dust samples comparable total iron contents in the range of 3.0 to 6.5 wt%, and they assigned a significant amount of 2.8 to 5.8% of this iron as present in iron oxide mineral phases. This result is consistent with the reported 2.8–5.0% of free iron in aerosol samples collected from three different locations over the world (Lafon et al., 2004; Lafon et al., 2006). Takahashi et al. (2011) indicated that the content of iron oxides is less than 5 wt% in Asian dust. Moreover, Klaver et al. (2011a) reported that the iron oxides-to-total iron ratio for the analysed samples varied between 0.4 and 0.61, accounting for between 1 and 3% of the total gravimetric mass, and Formenti et al. (2008) also illustrated that iron oxides (speciation hematite and goethite) represented 2.4 and 4.5% of the total mineral dust mass. As mentioned above, only about half of the total iron content is represented by free iron.

XRD (X-ray diffraction) analytical technology has also been applied to identify the content of hematite and goethite in some cases and less than 2% iron oxides were detected (Shi et al., 2005; Linke et al., 2006; Kandler et al., 2009; Lawrence et al., 2010; Klaver et al., 2011a; Wagner et al., 2012; Formenti et al., 2014b). Depending on the crystal phase of interest, this method has a detection limit of 0.1 to 0.5 wt% for iron oxides (Balsam et al., 2014). Discrepancies between the quantified free-iron content detected by the method of Lafon et al. (2006) and the hematite or goethite

contents determined by XRD could be due to difficulties of the Rietveld method associated with poor crystallographic ordering of iron oxides in mineral dusts.

Single particle analysis has also been conducted for detecting the free iron oxides. Fe-rich particles (iron oxides) represented no more than 5% of the particle number in aerosol samples and hematite or goethite were found more often in the fine fraction (Chou et al., 2008; Kandler et al., 2009; Schladitz et al., 2009; Kang et al., 2009; Scheuven et al., 2011; Malek et al., 2011; Wagner et al., 2012; Menéndez et al., 2014).

The technology of diffuse reflectance spectroscopy (DRS) has normally been to quantify the ratio of hematite to goethite in a particular dust sample (Lafon et al., 2006; Shen et al., 2006; Lázaro et al., 2008; Formenti et al., 2008). The accurate quantification of goethite and ferrihydrite in dust is extremely difficult owing to similarities in structure and associated absorption spectra of these two minerals (Scheinost et al., 1998; Torrent and Barrón, 2002; Schroth et al., 2009). This has the critical implication that the content of goethite measured by absorption spectroscopy is actually the sum of goethite and ferrihydrite. This does not, however, affect the optical calculations due to their optical similarity. Table 3 summarizes the measured ratios of hematite to goethite in global dust aerosol samples and shows higher ratios of Hm/Gt in Asian dust samples compared to African samples. Over the whole world, it is concluded that goethite predominates over hematite with a relative abundance of 50–75% of iron oxides in dust aerosols.

Based on the above reported results, we conclude that the iron oxides account for approximately half of the mass of elemental Fe and for between 2 and 5% of the dust mass. Most

Table 3. Summary of global reported ratios of hematite to goethite (Hm / Gt) in dust aerosols.

Location (number of samples)	Type	Method	Average value of Hm / Gt	Reference
Niger (1)	Aerosol ^a	DRS	0.5625	Lafon et al. (2006)
Tunisia (1)	Aerosol ^a	DRS	0.4085	Lafon et al. (2006)
China-Zhenbeitai (1)	Aerosol	DRS	0.3514	Lafon et al. (2006)
Niger (99)	Aerosol	DRS	0.4286	Formenti et al. (2008)
Niger (12)	Aerosol	XAS	0.5771	Formenti et al. (2014)
Gran Canaria (19)	Aerosol	DRS	0.9048	Lázaro et al. (2008)
North Atlantic (9)	Aerosol	DRS	0.9276	Arimoto et al. (2002)
Muztagata (7)	Aerosol	DRS	0.6918	Xu et al. (2014) ^b
Golmod (29)	Aerosol	DRS	0.7262	Yang et al. (2014)
Tazhong (6)	Aerosol	DRS	0.9157	Lu et al. (2011)
Dunhuang (29)	Aerosol	DRS	0.8762	Shen et al. (2006)
Yulin (32)	Aerosol	DRS	0.7158	Shen et al. (2006)
Horqin (22)	Aerosol	DRS	0.7448	Shen et al. (2006)
Australia (6)	Aerosol	MS	0.4571	Reynolds et al. (2014)

^a Dust aerosol produced by wind tunnel; ^b unpublished paper of T. L. Xu, private communication, 2014.

of them are composed of goethite, representing between 50 and 75 % of the iron oxide mass.

3.2.3 Mixing states

As free-iron particles are always mixed with other kinds of particle, the condition of the mixture could be important for their ability to scatter and absorb radiation. The 3-D structure of iron-oxide particles obtained by tomography reveals that these Fe-rich inclusions are often found at the surface of aluminosilicate particles but that some are also included inside particles (Deboudt et al., 2012). Inversions calculated assuming external mixing are better able to explain the wavelength dependence of dust absorption by varying only hematite concentration than inversions using internal mixing (Koven and Fung, 2006; Formenti et al., 2014a). Thus, a semi-external mixing assumption is clearly an optimal approximation for iron oxides mixed with aluminosilicate particles. Moreover, this assumption has the advantages of simplicity of calculation, interpretation and the possibility of comparing with model results.

3.3 Further simulation and verification

Sokolik and Toon (1999) also suggested that the radiative properties of a mixture would strongly depend on the relative abundance of individual minerals due to the large variations in the optical properties of individual minerals. Therefore, we model the optical properties for a range of possible weight fractions of hematite in the clay-size mode while the remaining mass is illite which represents the clay minerals. As mentioned above, we adopt 0 % hematite as the lower limit for the aerosol samples with no free-iron particles, 2.5 % hematite for the transported dust aerosol samples, 5 % hematite for the locally emitted dust samples and 7.5 % hematite for the

upper limit. Due to the limited and discontinuous refractive indices of goethite, this setting may underestimate the actual optical effects of goethite in dust aerosol. Using the density of hematite (5.3 g cm⁻³) and illite (2.75 g cm⁻³), volumetric hematite fraction was converted from the mass hematite fraction to calculate the effective complex refractive indices for dust.

Dust mineralogical composition is often expressed as a weighted fraction of individual components in the total dust sample. Because the relationship of number concentration and mass concentration can be expressed as

$$M_i = M_0 \cdot W_i = N_i \cdot \rho_i \cdot \frac{4}{3}\pi(r_0)^3 \cdot \exp\left[\frac{9}{2}(\ln \sigma)^2\right], \quad (3)$$

where M_i , N_i , W_i and ρ_i are the particle mass concentration, number concentration, weight fraction and density of the i th mineral in the mixture, respectively, and M_0 is the total particle mass concentration of the mixture sample, the optical properties of external mixtures of minerals can be modelled by

$$K_{\text{ext}}^{\text{mix}} = \sum (K_{\text{ext}(i)}^* \cdot N_i) = \sum \left(K_{\text{ext}(i)}^* \cdot \frac{M_0 \cdot W_i}{\rho_i \cdot \frac{4}{3}\pi(r_0)^3 \cdot \exp\left[\frac{9}{2}(\ln \sigma)^2\right]} \right). \quad (4)$$

Figure 4a shows the differences between the single-scattering albedo calculated for the mixture of illite and hematite with complex refractive indices from LG1988 at visible and infrared wavelengths. Compared to ω_0 for illite with no hematite, it is not hard to see that ω_0 for mixtures with different amount of hematite show significant differences in four wavelength ranges, namely, 0.2–0.7, 2.5–8.7, 8.7–12.5 and 15.0–17.5 μm . For $0.2 < \lambda < 0.7 \mu\text{m}$

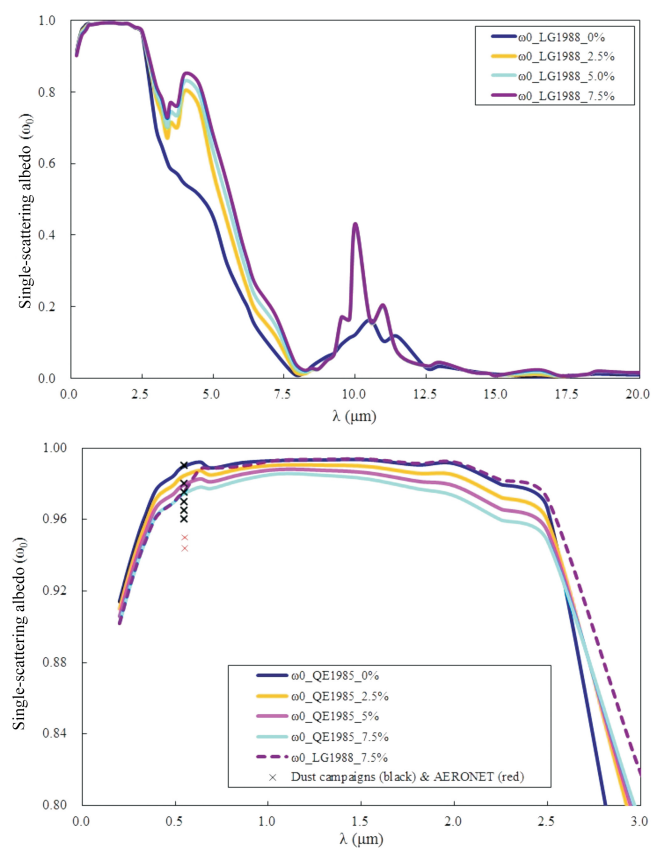


Figure 4. Spectral single-scattering albedo (SSA) for mixtures of illite and hematite with varying percentages and refractive indices at wavelengths of 0–20 μm (a) and 0–3 μm (b) with comparison to field observed results at 550 nm.

and $15.0 < \lambda < 17.5 \mu\text{m}$, ω_0 for the mixtures is smaller than ω_0 for pure illite, which means the presence of hematite enhances the optical absorption of the mixtures. For $2.5 < \lambda < 8.7 \mu\text{m}$, ω_0 for the mixtures is larger than for pure illite, which means the presence of hematite enhances the optical scattering of the mixtures. But for $8.7 < \lambda < 12.5 \mu\text{m}$, ω_0 shows more complicated fluctuations.

Figure 4b shows the differences between ω_0 for illite mixed with different amounts of hematite with refractive indices from QE1985 at solar wavelengths. The magnitude of ω_0 for a mixture increases when the median radius r_0 increases. In order to compare the effects for hematite with refractive indices from two different sources for the same mixture state, we also plot ω_0 for illite mixed with 7.5% hematite with refractive indices from LG1988 in Fig. 4b. Evidently, for $0.55 < \lambda < 2.5 \mu\text{m}$, the data set of QE1985 will lead to higher optical absorption, although the two data sets have the same optical scattering and absorption for $\lambda < 0.55 \mu\text{m}$.

Another coming question is what is the competition between theoretical calculated values and field observed results? In order to compare our calculated single-scattering albedos (SSAs) with measured values, we review all re-

ported SSAs during different dust campaigns or inferred from AERONET measurements, and listed them in Table 4. The measured results for dust mixed with BC were excluded during our review progress, such as the results from the campaign of the African Monsoon Multidisciplinary Analyses (AMMA). The measurements from the Dust and Biomass-burning Experiment (DABEX) are comparable but on the lower edge of previous measurements performed at 550 nm during the the Tropical Aerosol Radiative Forcing Observational Experiment (TARFOX), the Saharan Dust Experiment (SHADE), the Geostationary Earth Radiation Budget Intercomparison of Long-wave and Shortwave radiation experiment (GERBILS), the Saharan Mineral Dust Experiment (SAMUM), the NASA African Monsoon Multidisciplinary Analysis (NAMMA) and Fennec 2011 field campaigns. Absorption from the mineral dust as measured using the corrected nephelometer and particle soot absorption photometer (PSAP) combination suggests that single-scattering albedos at 550 nm (SSA550) range from 0.91 to 0.97 (with a mean of 0.97) for iron oxide mass fractions between 1.3 and 3.5% (Klaver et al., 2011a). The SSAs at 532 nm were reported as 0.99 ± 0.001 and 0.98 ± 0.002 for the Cairo 2 and Morocco dust samples with Fe_2O_3 mass fractions of 4.5 and 3.63%, respectively (Linke et al., 2006). Johnson and Osborne (2011) revealed that the use of the mineral dust refractive indices from Balkanski et al. (2007) assuming 1.5% hematite gave reasonable agreement with the measured single-scattering albedo, consistent with the findings of Klaver et al. (2011a). Haywood et al. (2011) showed that mineral dust is relatively non-absorbing at 550 nm due to the relatively small fraction of iron oxides present (1–3%). Balkanski et al. (2007) addressed this difference and argued that dust absorption at visible wavelengths might be lower than previously thought because mixing rule calculations with hematite content of 1.5% by volume, supposedly representative of median dust absorption, showed a very good agreement with the AERONET measurements. The same question is presented in Fig. 7a of Formenti et al. (2014a); that is, the calculated SSA using a higher imaginary index of iron oxides also overestimated the absorbing ability of Saharan dust in comparison with field observation.

We compare our calculated SSA curves with the measured values in Fig. 4b. It is shown that the observed SSAs mostly ranged in 0.94–0.99 during different dust campaigns, but much lower (0.944–0.95) for the AERONET which cannot exclude the presence of black carbon with higher absorbing. Our calculated result could be consistent with the higher part (0.97–0.99) of measured SSAs, but higher than the lower part (0.95–0.97) due to the effect of coarse particles during different dust campaigns. Thus, the iron oxide content alone cannot explain the variability of the single-scattering albedo. This suggests that more complete knowledge of the dust mineralogical composition and size distribution with varied multi-modes is needed as input to more rigorous modelling.

Table 4. Review of measured dust single-scattering albedos during dust campaigns and AERONET observations.

References	SSA _{550 nm} (Mean)	SD	Observations
Haywood et al. (2001)	0.97	0.02	TARFOX
Haywood et al. (2003)	0.97	0.02	SHADE
Johnson and Osborne (2011)	0.97	0.02	GERBILS
Müller et al. (2011)	0.96	0.03	SAMUM_2
Petzold et al. (2011)	0.975	0.15	SAMUM
Jeong et al. (2008)	0.96	0.01	NAMMA
Osborne et al. (2008)	0.99	0.02	DABEX
Ryder et al. (2013)	0.965	0.015	Fennec 2011
Lack et al. (2009)	0.95	0.01	TexAQS/GoMACCS
Linke et al. (2006)	0.985	0.006	Laboratory
Zhu et al. (2007)	0.95	0.01	AERONET
Kim et al. (2011)	0.944	0.005	AERONET

In order to check the further effects of the mixing state of hematite on the single-scattering albedo, we use two sets of assumptions that bracket the actual state of hematite mixing: internal mixing (Int), in which individual dust particles are a combination of all components present; and external mixing (Ext), in which different components exist as separate particles.

For the case of an external mixture of particles, the average optical properties are calculated by summing over the optical properties of the individual species. Approximations have to be made to calculate the optical properties of internal mixed particles. Three common approximations for the calculation of these latter optical properties are the volume mixing method, the Bruggeman approximation and the Maxwell–Garnett approximation (Chyýlek et al., 1988; Bohren and Huffman, 1998). Detail information about the three methods is given by Sokolik and Toon (1999). We have calculated the SSA of illite–hematite mixtures with different hematite contents using internal mixing according to the above three internal approximations and also using external mixing.

The calculated SSA values for illite–hematite mixtures using internal and external mixture assumptions as a function of wavelength and hematite mass fraction are illustrated in Fig. 5. For the case of external mixing, the SSAs at 405 nm show good agreement for refractive indices from QE1985 and LG1988, but the calculated SSAs at 870 nm for hematite with refractive indices from QE1985 are much smaller than those using LG1988. This is explained by Fig. 4b where the two data sets have the same optical scattering and absorbing properties for $\lambda < 0.55 \mu\text{m}$ but the data set of QE1985 leads to higher optical absorption for $\lambda > 0.55 \mu\text{m}$. The calculated SSAs with the three different internal mixing methods are all much smaller than those for external mixing both at 405 and 870 nm since the assumption of an external mixture results in less absorption and less wavelength dependence of absorption than does the assumption of an internal mixture for small amounts of hematite. The basic reason for this

is due to the extremely high imaginary refractive index for hematite at short wavelengths. For the case of internal mixing, the SSAs from the volume mixing method are smaller than for the other methods. This is due to the averaged imaginary refractive index being larger than for the other two approximations. On the basis of the study of Peterson (1968), only the effective refractive index of the non-metallic part of the dust can be calculated using the volume mixing method. Thus, adopting the volume mixing method to calculate the optical properties of aerosol samples will lead to a smaller SSA (Levoni et al., 1997; Sokolik and Toon, 1999; Shi et al., 2005; Höller et al., 2003; Ebert et al., 2004; Kandler et al., 2007; Kandler et al., 2009; Petzold et al., 2009; Otto et al., 2009; Wagner et al., 2012).

The calculated SSAs using the Bruggeman approximation are consistent with those from the Maxwell–Garnet approximation for low hematite contents at both 405 nm and 870 nm but differ from them for hematite content larger than 10%. Both the Maxwell–Garnet and Bruggeman approximations are derived from the same integral equation for the propagation of electromagnetic waves in an inhomogeneous medium but under a different set of approximations (Chyýlek et al., 1988; Bohren and Huffman, 1998). In previous studies, the Bruggeman approximation (Sokolik and Toon, 1999; Lafon et al., 2006; Koven and Fung, 2006; Mishra and Tripathi, 2008; Thomas and Gautier, 2009; McConnell et al., 2010; Klaver et al., 2011a; Wagner et al., 2012; Mishra et al., 2012) has been more often used for calculating the complex refractive index of silicate–hematite mixtures than the Maxwell–Garnet approximations (Balkanski et al., 2007; Hansell Jr. et al., 2011).

The Bruggeman approximation allows for the calculation of an effective dielectric constant of multicomponent mixtures without distinguishing between matrix and inclusions. If we do not know which is the main body for the silicate and the hematite in an aerosol, it is better to choose the Bruggeman approximation. For the Maxwell–Garnet approx-

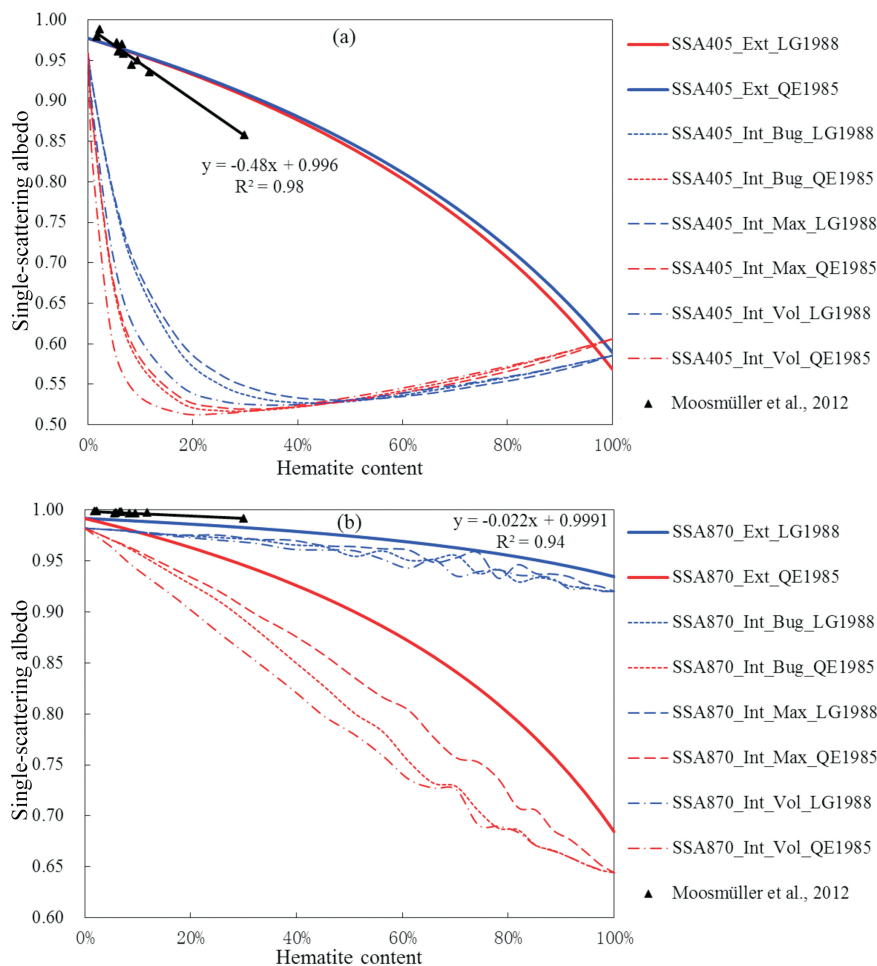


Figure 5. The single-scattering albedo (SSA) as a function of varying hematite content at wavelengths of (a) 405 and (b) 870 nm, with different mixing states (internal and external mixing), different complex refractive index sources (QE1985 and LG1988) and mixing approximations (volume, Maxwell–Garnet and Bruggeman). For comparison, the measured values using a photoacoustic instrument with integrating reciprocal nephelometer and linear fits from Moosmüller et al. (2012) are also shown.

imation, a decision must be made as to which component is the matrix and which is an inclusion. The Maxwell–Garnett approximation is designed for small inclusions inside a host matrix and thus it is not suitable for hematite > 50 % in the mixture, so the calculated SSAs show abnormal fluctuation for hematite > 50 % in Fig. 5. This phenomenon disappears if we consider the inverse Maxwell–Garnet approximation which makes hematite the host matrix. Actually, the variation of Fe_2O_3 has been constrained within the range 0–10 %, so we advise the use of the Maxwell–Garnet approximation in which the inclusions should be identical in composition but may be different in volume, shape and orientation.

The comparison between the laboratories measured SSAs with known abundance of iron oxides with our theoretically calculated SSAs by different mixing rules, would give us further insights into the actual mixing states of iron oxides and accuracy of different refractive indices. Laboratory measured SSAs by extinction and photoacoustic absorption measure-

ments at different wavelengths have been reported in Linke et al. (2006) and Moosmüller et al. (2012). Moosmüller et al. (2012) have demonstrated that SSAs are much smaller at 405 nm than at 870 nm and that SSAs at both wavelengths are dominated by and linearly correlated with the iron content. These measured results are also shown in Fig. 5 for comparison with our theoretically calculated SSAs. The measured SSAs at 405 nm show good agreement with our external mixing SSA values calculated from both LG1988 and QE1985 for hematite less than 10 %, while they are much larger than our internal mixing SSA values at 405 nm (Fig. 5a), potentially indicating that the dust samples are mainly external mixing and are accompanied by a very small degree of internal mixing.

In contrast, the measured SSA values at 870 nm are much larger than our external and internal mixing SSA values calculated from refractive indices from QE1985 but show good agreement with our external mixing SSA values calculated

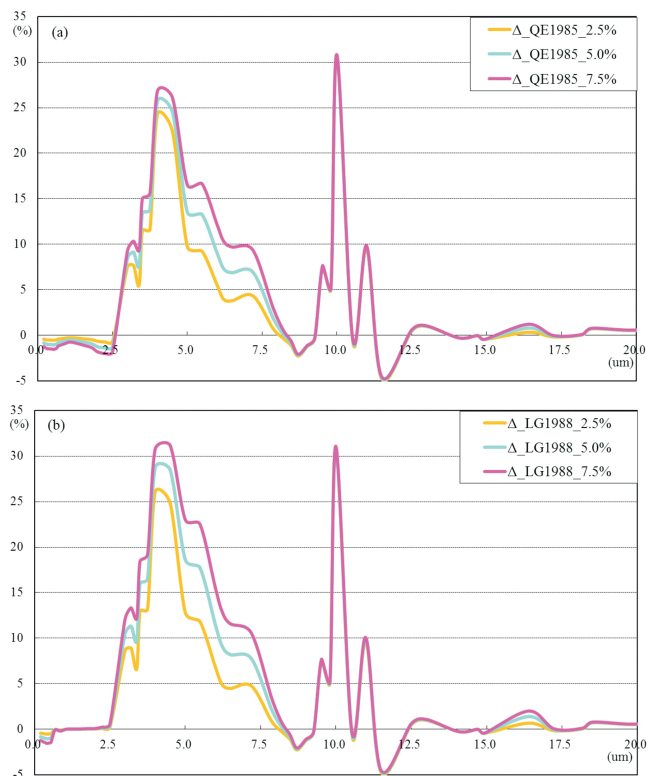


Figure 6. The difference $\Delta\omega_0$ between the single-scattering albedo (SSA) of pure illite and the single-scattering albedo of mixtures with different contents and refractive indices of hematite. (a) Complex refractive index of hematite from Query (1985), (b) complex refractive index of hematite from Longtin (1988).

using LG1988 values (Fig. 5b). This illustrates the fact that the complex refractive indices of hematite from QE1985 have greatly overestimated absorption at 870 nm.

For purposes of quantitatively illustrating the optical effects of hematite in the mixtures, we calculate $\Delta\omega_0$ as the difference between the single-scattering albedo of mixtures with given abundances of hematite and pure illite. Thus, we have

$$\Delta\omega_0 = \frac{\omega_0^{\text{mixture}} - \omega_0^{\text{illite}}}{\omega_0^{\text{illite}}} \times 100\% \quad (5)$$

Here, we assume $M_0 = 100 \mu\text{g cm}^{-3}$ and a lognormal size distribution with $r_0 = 0.5 \mu\text{m}$, $\sigma = 2.0$. The single-scattering albedo of pure illite represents the case when the dust contains no hematite. If the calculated values of $\Delta\omega_0$ are negative, this means that hematite has high absorption at the corresponding wavelengths. Figure 6 shows $\Delta\omega_0$ calculated for hematite with refractive indices from QE1985 and LG1988 at $\lambda < 20 \mu\text{m}$. It demonstrates that hematite with refractive indices from LG1988 only enhances the optical absorption of dust mixtures for $\lambda < 0.55 \mu\text{m}$, but hematite with refractive indices from QE1985 enhances the absorption for $\lambda < 2.5 \mu\text{m}$. The magnitude of $\Delta\omega_0$ for 5% hematite over

these wavelengths is approximately about 1%. Therefore, the use of refractive indices for hematite from QE1985 in climate models would lead to overestimation of the optical absorption at both visible and near-IR wavelengths. Another apparent difference is the positive magnitude of $\Delta\omega_0$ for hematite with refractive indices from the two data sets at wavelengths of $2.5 < \lambda < 8.7 \mu\text{m}$.

Given all that, the complex refractive index of iron oxides is therefore a key parameter in effects of dust aerosols on the radiation balance, and the optical constants of hematite from different sources become a major source of uncertainty in radiative forcing calculation. Further work is needed to provide experimental measurements of the refractive index of iron oxides, especially for hematite and goethite in the visible region of the spectrum. More complete knowledge of the dust mineralogy, morphology and size distribution with varied multi-modes is needed as input to more rigorous modelling.

4 Summary

In this paper we have investigated the spectral optical properties of iron oxides with considering different refractive indices, size distributions and more logical weight fractions and mixing states of iron oxides. The iron oxides account for approximately half of the mass of elemental Fe and for between 2 and 5% of the dust mass. Most of them are composed of goethite, representing between 50 and 75% of the iron oxide mass. The iron oxides commonly occur as spheroidal to ellipsoidal nanoparticles that may be single or aggregated, and may be unattached or attached to quartz or clay minerals, which could be expressed as semi-external mixing state. Moreover, the spectral SSA values determined in the present study show a strong wavelength dependence with a steep decrease from the visible to the near-UV. There are still problems that need to be solved in order to accurately study the real role of iron oxides in determining the overall impact of dust aerosols on climate perturbation, as follows:

1. Although there have been many published investigations of the complex refractive index of different iron oxides, uniformly continuous optical constants for a single type of iron oxides from 0.2 to $50 \mu\text{m}$ are very scarce. Some of them are inconsistent and careful checking of their accuracy is therefore essential.
2. The abundance of specific iron-oxide types (such as goethite and magnetite) remains unknown. Although many studies have measured the mass ratio of goethite to hematite as about 7 : 3, the absence of goethite optical constants at 0.75–8.5 μm restricts the usefulness of this ratio. Thus, using hematite to represent all types of iron oxides is a popular hypothesis.
3. Microscopic observations and optical simulations have shown that semi-external mixtures employing both ex-

ternal mixtures of Fe aggregates and other minerals and partly internal mixing between iron oxides and aluminosilicate particles is the optimal mixing approximation.

4. For hematite, there are two data sets of complex refractive indices that differ significantly. Compared with LG1988, the complex refractive indices of QE1985 greatly overestimate the optical absorption at both visible and near-IR wavelengths. Comprehensive laboratory measurements of the refractive indices of iron oxides, especially of hematite and goethite in the visible spectrum, should therefore be made in order to accurately assess the effect of mineral dust on climate perturbation.

Theoretically, calculated SSA values are comparable to values observed in recent laboratory and field studies in the range of 0.97–0.99. The iron oxide content alone cannot explain the variability of the single-scattering albedo, and the lower SSAs could be explained as the presence of coarse dust particles and high-absorbing black carbon in natural transported dust aerosol. More complete knowledge of the dust mineralogical composition and size distribution with dynamic varied multi-modes is needed as input to more rigorous modelling. Furthermore, field observations focus on the mean and standard deviations of the modes for various sources, surface wind speeds and transport meteorology should also be conducted.

Acknowledgements. We are grateful to Yahui Yue at ITPCAS and Yongliang Li at BNU for completing the SEM–EDX analysis and Michael Mishchenko at NASA GISS for offering the T-matrix and Lorenz–Mie codes. We are also grateful for the helpful comments made by the editor David Covert, the reviewer Yves Balkanski and another anonymous reviewer. This work was supported by the National Natural Science Foundation of China (grant no. 41205108, 41571063 and 41271074).

Edited by: D. Covert

References

Alfaro, S., Lafon, S., Rajot, J., Formenti, P., Gaudichet, A., and Maille, M.: Iron oxides and light absorption by pure desert dust: an experimental study, *J. Geophys. Res.-Atmos.*, 109, D08208, doi:10.1029/2003JD004374, 2004.

Anderson, B. and Jenne, E.: Free-iron and-manganese oxide content of reference clays, *Soil Sci.*, 109, 163–169, 1970.

Angel, B. and Vincent, W.: Associated with the surface of kaolins, *Clay Miner.*, 26, 263–272, 1978.

Arimoto, R., Ray, B., Lewis, N., Tomza, U., and Duce, R.: Mass-particle size distributions of atmospheric dust and the dry deposition of dust to the remote ocean, *J. Geophys. Res.-Atmos.*, 102, 15867–15874, 1997.

Arimoto, R., Balsam, W., and Schloesslin, C.: Visible spectroscopy of aerosol particles collected on filters: iron-oxide minerals, *Atmos. Environ.*, 36, 89–96, 2002.

Balkanski, Y., Schulz, M., Claquin, T., and Guibert, S.: Reevaluation of Mineral aerosol radiative forcings suggests a better agreement with satellite and AERONET data, *Atmos. Chem. Phys.*, 7, 81–95, doi:10.5194/acp-7-81-2007, 2007.

Balsam, W., Ji, J., Renock, D., Deaton, B. C., and Williams, E.: Determining hematite content from NUV/Vis/NIR spectra: limits of detection, *Am. Mineral.*, 99, 2280–2291, 2014.

Baltrusaitis, J., Cwiertny, D. M., and Grassian, V. H.: Adsorption of sulfur dioxide on hematite and goethite particle surfaces, *Phys. Chem. Chem. Phys.*, 9, 5542–5554, 2007.

Bedidi, A. and Cervelle, B.: Light scattering by spherical particles with hematite and goethitelike optical properties: effect of water impregnation, *J. Geophys. Res.-Sol. Ea.*, 98, 11941–11952, 1993.

Bohren, C. F. and Huffman, D. R.: *Absorption and Scattering of Light by Small Particles*, John Wiley and Sons, New York, 1998.

Chiappello, I., Bergametti, G., Chatenet, B., Bousquet, P., Dulac, F., and Soares, E. S.: Origins of African dust transported over the northeastern tropical Atlantic, *J. Geophys. Res.-Atmos.*, 102, 13701–13709, doi:10.1029/97JD00259, 1997.

Chou, C., Formenti, P., Maille, M., Ausset, P., Helas, G., Harrison, M., and Osborne, S.: Size distribution, shape, and composition of mineral dust aerosols collected during the African monsoon multidisciplinary analysis special observation period 0: dust and biomass – burning experiment field campaign in Niger, January 2006, *J. Geophys. Res.-Atmos.*, 113, D00C10, doi:10.1029/2008JD009897, 2008.

Chyýlek, P., Srivastava, V., Pinnick, R. G., and Wang, R.: Scattering of electromagnetic waves by composite spherical particles: experiment and effective medium approximations, *Appl. Optics*, 27, 2396–2404, 1988.

Claquin, T., Schulz, M., Balkanski, Y. J.: Modeling the mineralogy of atmospheric dust sources, *J. Geophys. Res.-Atmos.*, 104, 22243–22256, doi:10.1029/1999JD900416, 1999.

Cornell, R. M. and Schwertmann, U.: *The Iron Oxides: Structure, Properties, Reactions, Occurrences and Uses*, John Wiley and Sons, New York, 2006.

Dang, C. and Hegg, D. A.: Quantifying light absorption by organic carbon in western North American snow by serial chemical extractions, *J. Geophys. Res.-Atmos.*, 119, 10247–10261, 2014.

Dave, J. and Center, I. P. A. S.: *Subroutines for Computing the Parameters of the Electromagnetic Radiation Scattered by a Sphere*, IBM Scientific Center, Palo Alto, California, 1968.

Deboudt, K., Gloter, A., Mussi, A., and Flament, P.: Red-speciation and mixing state of iron in individual African dust particles, *J. Geophys. Res.-Atmos.*, 117, D12307, doi:10.1029/2011JD017298, 2012.

Derimian, Y., Karnieli, A., Kaufman, Y. J., Andreae, M. O., Andreae, T. W., Dubovik, O., Maenhaut, W., and Koren, I.: The role of iron and black carbon in aerosol light absorption, *Atmos. Chem. Phys.*, 8, 3623–3637, doi:10.5194/acp-8-3623-2008, 2008.

Dupart, Y., King, S. M., Nekat, B., Nowak, A., Wiedensohler, A., Herrmann, H., David, G., Thomas, B., Miffre, A., and Rairoux, P.: Mineral dust photochemistry induces nucleation events in the

- presence of SO₂, *P. Natl. Acad. Sci. USA*, 109, 20842–20847, 2012.
- Ebert, M., Weinbruch, S., Hoffmann, P., and Ortner, H. M.: The chemical composition and complex refractive index of rural and urban influenced aerosols determined by individual particle analysis, *Atmos. Environ.*, 38, 6531–6545, 2004.
- Formenti, P., Rajot, J. L., Desboeufs, K., Caquineau, S., Chevaillier, S., Nava, S., Gaudichet, A., Journet, E., Triquet, S., and Alfaro, S.: Regional variability of the composition of mineral dust from western Africa: results from the AMMA SOP0/DABEX and DODO field campaigns, *J. Geophys. Res.-Atmos.*, 113, D00C13, doi:10.1029/2008JD009903, 2008.
- Formenti, P., Schütz, L., Balkanski, Y., Desboeufs, K., Ebert, M., Kandler, K., Petzold, A., Scheuvens, D., Weinbruch, S., and Zhang, D.: Recent progress in understanding physical and chemical properties of African and Asian mineral dust, *Atmos. Chem. Phys.*, 11, 8231–8256, doi:10.5194/acp-11-8231-2011, 2011.
- Formenti, P., Caquineau, S., Chevaillier, S., Klaver, A., Desboeufs, K., Rajot, J., Belin, S., and Briois, V.: Dominance of goethite over hematite in iron oxides of mineral dust from Western Africa: quantitative partitioning by X-ray absorption spectroscopy, *J. Geophys. Res.-Atmos.*, 119, 12740–12754, doi:10.1002/2014JD021668, 2014a.
- Formenti, P., Caquineau, S., Desboeufs, K., Klaver, A., Chevaillier, S., Journet, E., and Rajot, J. L.: Mapping the physico-chemical properties of mineral dust in western Africa: mineralogical composition, *Atmos. Chem. Phys.*, 14, 10663–10686, doi:10.5194/acp-14-10663-2014, 2014b.
- Galuzza, A., Eremenko, V., and Kirichenko, A.: Analysis of hematite reflection spectrum by the Kramers-Kronig method, *Sov. Phys.-Sol. State*, 21, 654–656, 1979.
- Ganor, E. and Foner, H.: The mineralogical and chemical properties and the behaviour of aeolian Saharan dust over Israel, in: *The Impact of Desert Dust Across the Mediterranean*, Springer, Kluwer Academic Publishers, Dordrecht, the Netherlands, 163–172, 1996.
- Gao, Y., Kaufman, Y., Tanre, D., Kolber, D., and Falkowski, P.: Seasonal distributions of aeolian iron fluxes to the global ocean, *Geophys. Res. Lett.*, 28, 29–32, 2001.
- Gillespie, J. B. and Lindberg, J. D.: Ultraviolet and visible imaginary refractive index of strongly absorbing atmospheric particulate matter, *Appl. Optics*, 31, 2112–2115, 1992.
- Ginot, P., Dumont, M., Lim, S., Patris, N., Taupin, J.-D., Wagnon, P., Gilbert, A., Arnaud, Y., Marinoni, A., Bonasoni, P., and Laj, P.: A 10 year record of black carbon and dust from a Mera Peak ice core (Nepal): variability and potential impact on melting of Himalayan glaciers, *The Cryosphere*, 8, 1479–1496, doi:10.5194/tc-8-1479-2014, 2014.
- Glotch, T. D. and Rogers, A. D.: Evidence for aqueous deposition of hematite- and sulfate- rich 30 light-toned layered deposits in Aureum and Iani Chaos, Mars, *J. Geophys. Res.-Planet.*, 112, E06001, doi:10.1029/2006JE002863, 2007.
- Glotch, T. D. and Rossman, G. R.: Mid-infrared reflectance spectra and optical constants of six iron oxide/oxyhydroxide phases, *Icarus*, 204, 663–671, 2009.
- Gomes, L. and Gillette, D. A.: A comparison of characteristics of aerosol from dust storms in central Asia with soil-derived dust from other regions, *Atmos. Environ. A-Gen.*, 27, 2539–2544, 1993.
- Greenland, D. J., Oades, J., and Sherwin, T.: Electron-microscope observations of iron oxides in some red soils, *J. Soil Sci.*, 19, 123–126, 1968.
- Guieu, C., Loÿe-Pilot, M. D., Ridame, C., and Thomas, C.: Chemical characterization of the Saharan dust end-member: some biogeochemical implications for the western Mediterranean Sea, *J. Geophys. Res.-Atmos.*, 107, ACH 5-1–ACH 5-11, 2002.
- Guo, H. and Barnard, A. S.: Naturally occurring iron oxide nanoparticles: morphology, surface chemistry and environmental stability, *J. Mater. Chem.*, 1, 27–42, 2013.
- Hansell Jr., R. A., Reid, J. S., Tsay, S. C., Roush, T. L., and Kalashnikova, O. V.: A sensitivity study on the effects of particle chemistry, asphericity and size on the mass extinction efficiency of mineral dust in the earth's atmosphere: from the near to thermal IR, *Atmos. Chem. Phys.*, 11, 1527–1547, doi:10.5194/acp-11-1527-2011, 2011.
- Haywood, J., Francis, P., Glew, M., and Taylor, J.: Optical properties and direct radiative effect of Saharan dust: A case study of two Saharan dust outbreaks using aircraft data, *J. Geophys. Res.-Atmos.*, 106, 18417–18430, doi:10.1029/2000JD900319, 2001.
- Haywood, J., Francis, P., Osborne, S., Glew, M., Loeb, N., Highwood, E., Tanré, D., Myhre, G., Formenti, P., and Hirst, E.: Radiative properties and direct radiative effect of Saharan dust measured by the C-130 aircraft during SHADE: 1. Solar spectrum, *J. Geophys. Res.-Atmos.*, 108, 8577, doi:10.1029/2002JD002687, 2003.
- Haywood, J., Johnson, B., Osborne, S., Baran, A., Brooks, M., Milton, S., Mulcahy, J., Walters, D., Allan, R., and Klaver, A.: Motivation, rationale and key results from the GERBILS Saharan dust measurement campaign, *Q. J. Roy. Meteor. Soc.*, 137, 1106–1116, 2011.
- Henning, T. and Mutschke, H.: Low-temperature infrared properties of cosmic dust analogues, *Astron. Astrophys.*, 327, 743–754, 1997.
- Henning, T., Begemann, B., Mutschke, H., and Dorschner, J.: Optical properties of oxide dust grains, *Astron. Astrophys. Sup.*, 112, 143–149, 1995.
- Hinds, W. C.: *Aerosol Technology: Properties, Behavior, and Measurement of Airborne Particles*, Wiley-Interscience, New York, 442 pp., 1982.
- Höller, R., Ito, K., Tohno, S., and Kasahara, M.: Wavelength-dependent aerosol singlescattering albedo: measurements and model calculations for a coastal site near the Sea of Japan during ACE-Asia, *J. Geophys. Res.-Atmos.*, 108, 8648, doi:10.1029/2002JD003250, 2003.
- Hsu, W. P. and Matijević, E.: Optical properties of monodispersed hematite hydrosols, *Appl. Optics*, 24, 1623–1630, 1985.
- Jeong, M. J., Tsay, S. C., Ji, Q., Hsu, N. C., Hansell, R. A., and Lee, J.: Ground-based measurements of airborne Saharan dust in marine environment during the NAMMA field experiment, *Geophys. Res. Lett.*, 35, L20805, doi:10.1029/2008GL035587, 2008.
- Jickells, T., An, Z., Andersen, K. K., Baker, A., Bergametti, G., Brooks, N., Cao, J., Boyd, P., Duce, R., and Hunter, K.: Global iron connections between desert dust, ocean biogeochemistry, and climate, *Science*, 308, 67–71, 2005.
- Johnson, B. and Osborne, S.: Physical and optical properties of mineral dust aerosol measured by aircraft during the GERBILS campaign, *Q. J. Roy. Meteor. Soc.*, 137, 1117–1130, 2011.

- Journet, E., Balkanski, Y., and Harrison, S. P.: A new data set of soil mineralogy for dust-cycle modeling, *Atmos. Chem. Phys.*, 14, 3801–3816, doi:10.5194/acp-14-3801-2014, 2014.
- Kandler, K., Benker, N., Bundke, U., Cuevas, E., Ebert, M., Knippertz, P., Rodríguez, S., Schütz, L., and Weinbruch, S.: Chemical composition and complex refractive index of Saharan Mineral Dust at Izana, Tenerife (Spain) derived by electron microscopy, *Atmos. Environ.*, 41, 8058–8074, 2007.
- Kandler, K., Schütz, L., Deutscher, C., Ebert, M., Hofmann, H., Jäckel, S., Jaenicke, R., Knippertz, P., Lieke, K., and Massling, A.: Size distribution, mass concentration, chemical and mineralogical composition and derived optical parameters of the boundary layer aerosol at Tinfou, Morocco, during SAMUM 2006, *Tellus B*, 61, 32–50, 2009.
- Kandler, K., Lieke, K., Benker, N., Emmel, C., Küpper, M., Müller-Ebert, D., Ebert, M., Scheuven, D., Schladitz, A., and Schütz, L.: Electron microscopy of particles collected at Praia, Cape Verde, during the Saharan mineral dust experiment: particle chemistry, shape, mixing state and complex refractive index, *Tellus B*, 63, 475–496, 2011.
- Kang, S., Hwang, H., Kang, S., Park, Y., Kim, H., and Ro, C.-U.: Quantitative ED-EPMA combined with morphological information for the characterization of individual aerosol particles collected in Incheon, Korea, *Atmos. Environ.*, 43, 3445–3453, 2009.
- Kaspari, S., Painter, T. H., Gysel, M., Skiles, S. M., and Schwikowski, M.: Seasonal and elevational variations of black carbon and dust in snow and ice in the Solu-Khumbu, Nepal and estimated radiative forcings, *Atmos. Chem. Phys.*, 14, 8089–8103, doi:10.5194/acp-14-8089-2014, 2014.
- Kerker, M., Scheiner, P., Cooke, D., and Kratochvil, J.: Absorption index and color of colloidal hematite, *J. Colloid Interf. Sci.*, 71, 176–187, 1979.
- Kim, D., Chin, M., Yu, H., Eck, T. F., Sinyuk, A., Smirnov, A., and Holben, B. N.: Dust optical properties over North Africa and Arabian Peninsula derived from the AERONET dataset, *Atmos. Chem. Phys.*, 11, 10733–10741, doi:10.5194/acp-11-10733-2011, 2011.
- Klaver, A., Formenti, P., Caquineau, S., Chevaillier, S., Ausset, P., Calzolari, G., Osborne, S., Johnson, B., Harrison, M., and Dubovik, O.: Physico-chemical and optical properties of Sahelian and Saharan mineral dust: in situ measurements during the GERBILS campaign, *Q. J. Roy. Meteor. Soc.*, 137, 1193–1210, 2011a.
- Klaver, Y., Lemmens, V., Creemers, G., Rutten, H., Nienhuijs, S., and de Hingh, I.: Populationbased survival of patients with peritoneal carcinomatosis from colorectal origin in the era of increasing use of palliative chemotherapy, *Ann. Oncol.*, 22, 2250–2256, 2011b.
- Köhler, C. H., Trautmann, T., Lindermeier, E., Vreeling, W., Lieke, K., Kandler, K., Weinzierl, B., Groß, S., Tesche, M., and Wendisch, M.: Thermal IR radiative properties of mixed mineral dust and biomass aerosol during SAMUM-2, *Tellus B*, 63, 751–769, 2011.
- Koven, C. D. and Fung, I.: Inferring dust composition from wavelength-dependent absorption in Aerosol Robotic Network (AERONET) data, *J. Geophys. Res.-Atmos.*, 111, D14205, doi:10.1029/2005JD006678, 2006.
- Krekov, G. M.: Models of atmospheric aerosols, in: *Aerosol Effects on Climate*, edited by: Jennings, S. G., Univ. of Ariz. Press, Tucson, 9–72, 1992.
- Lack, D. A., Quinn, P. K., Massoli, P., Bates, T. S., Coffman, D., Covert, D. S., Sierau, B., Tucker, S., Baynard, T., Lovejoy, E., Murphy, D. M., and Ravishankara, A. R.: Relative humidity dependence of light absorption by mineral dust after long-range atmospheric transport from the Sahara, *Geophys. Res. Lett.*, 36, L24805, doi:10.1029/2009GL041002, 2009.
- Lafon, S., Sokolik, I., Rajot, J., Caquineau, S., and Gaudichet, A.: Characterization of iron oxides in mineral dust aerosols: Implications for light absorption, *J. Geophys. Res.*, 111, D21207, doi:10.1029/2005JD007016, 2006.
- Lafon, S., Rajot, J.-L., Alfaro, S. C., and Gaudichet, A.: Quantification of iron oxides in desert aerosol, *Atmos. Environ.*, 38, 1211–1218, 2004.
- Lawrence, C. R., Painter, T., Landry, C., and Neff, J.: Contemporary geochemical composition and flux of aeolian dust to the San Juan Mountains, Colorado, United States, *J. Geophys. Res.-Biogeo.*, 115, G03007, doi:10.1029/2009JG001077, 2010.
- Lázaro, F. J., Gutiérrez, L., Barrón, V., and Gelado, M. D.: The speciation of iron in desert dust collected in Gran Canaria (Canary Islands): combined chemical, magnetic and optical analysis, *Atmos. Environ.*, 42, 8987–8996, 2008.
- Levoni, C., Cervino, M., Guzzi, R., and Torricella, F.: Atmospheric aerosol optical properties: a database of radiative characteristics for different components and classes, *Appl. Optics*, 36, 8031–8041, 1997.
- Liao, H. and Seinfeld, J. H.: Radiative forcing by mineral dust aerosols: sensitivity to key variables, *J. Geophys. Res.-Atmos.*, 103, 31637–31645, doi:10.1029/1998JD200036, 1998.
- Linke, C., Möhler, O., Veres, A., Mohácsi, Á., Bozóki, Z., Szabó, G., and Schnaiter, M.: Optical properties and mineralogical composition of different Saharan mineral dust samples: a laboratory study, *Atmos. Chem. Phys.*, 6, 3315–3323, doi:10.5194/acp-6-3315-2006, 2006.
- Longtin, D. R., Shettle, E. P., Hummel, J. R., and Pryce, J. D.: A Wind Dependent Desert Aerosol Model: Radiative Properties, Air Force Geophys. Lab., Air Force Syst. Command Hanscom Air Force Base, Mass, AFGL-TR-88-0112, 115, 1988.
- Lu, H., Wei, W., Liu, M., Wu, X., Mou, S., and Han, Q.: Quantification and semi-quantification of iron-oxide minerals in aerosol particles in the hinterland of Taklimakan Desert, *Scientia Geographica Sinica*, 31, 969–975, 2011.
- Mahowald, N., Albani, S., Kok, J. F., Engelstaeder, S., Scanza, R., Ward, D. S., and Flanner, M. G.: The size distribution of desert dust aerosols and its impact on the Earth system, *Aeolian Res.*, 15, 53–71, 2013.
- Malek, M. A., Kim, B., Jung, H.-J., Song, Y.-C., and Ro, C.-U.: Single-particle mineralogy of Chinese soil particles by the combined use of low-Z particle electron probe X-ray microanalysis and attenuated total reflectance-FT-IR imaging techniques, *Anal. Chem.*, 83, 7970–7977, 2011.
- Marra, A., Blanco, A., Fonti, S., Jurewicz, A., and Orofino, V.: Fine hematite particles of Martian interest: absorption spectra and optical constants, *J. Phys. Conf. Ser.*, 6, 132–138, 2005.
- McConnell, C. L., Formenti, P., Highwood, E. J., and Harrison, M. A. J.: Using aircraft measurements to determine the refractive index of Saharan dust during the DODO Experiments, At-

- mos. Chem. Phys., 10, 3081–3098, doi:10.5194/acp-10-3081-2010, 2010.
- Meland, B., Kleiber, P., Grassian, V., and Young, M.: Visible light scattering study at 470, 550, and 660 nm of components of mineral dust aerosol: hematite and goethite, *J. Quant. Spectrosc. Ra.*, 112, 1108–1118, 2011.
- Menéndez, I., Pérez-Chacón, E., Mangas, J., Tauler, E., Engelbrecht, J. P., Derbyshire, E., Cana, L., and Alonso, I.: Dust deposits on La Graciosa Island (Canary Islands, Spain): texture, mineralogy and a case study of recent dust plume transport, *Catena*, 117, 133–144, 2014.
- Mishchenko, M. I., Travis, L. D., and Lacis, A. A.: Scattering, Absorption, and Emission of Light by Small Particles, Cambridge University Press, 2002.
- Mishra, S. K. and Tripathi, S. N.: Modeling optical properties of mineral dust over the Indian Desert, *J. Geophys. Res.-Atmos.*, 113, D23201, doi:10.1029/2008JD010048, 2008.
- Mishra, S. K., Tripathi, S. N., Aggarwal, S. G., and Arola, A.: Optical properties of accumulation mode, polluted mineral dust: effects of particle shape, hematite content and semi-external mixing with carbonaceous species, *Tellus B*, 64, 18536, doi:10.3402/tellusb.v64i0.18536, 2012.
- Moosmüller, H., Engelbrecht, J. P., Skiba, M., Frey, G., Chakrabarty, R. K., and Arnott, W. P.: Single scattering albedo of fine mineral dust aerosols controlled by iron concentration, *J. Geophys. Res.-Atmos.*, 117, D11210, doi:10.1029/2011JD016909, 2012.
- Mukai, T.: Cometary dust and interplanetary particles, in: *Evolution of Interstellar Dust and Related Topics*, Elsevier Science, Amsterdam, 397–445, 1989.
- Müller, T., Schladitz, A., Massling, A., Kaaden, N., Kandler, K., and Wiedensohler, A.: Spectral absorption coefficients and imaginary parts of refractive indices of Saharan dust during SAMUM-1, *Tellus B*, 61, 79–95, 2009.
- Müller, T., Schladitz, A., Kandler, K., and Wiedensohler, A.: Spectral particle absorption coefficients, single scattering albedos and imaginary parts of refractive indices from ground based in situ measurements at Cape Verde Island during SAMUM-2, *Tellus B*, 63, 573–588, 2011.
- Muñoz, O., Volten, H., Hovenier, J., Min, M., Shkuratov, Y. G., Jalava, J., Van der Zande, W., and Waters, L.: Experimental and computational study of light scattering by irregular particles with extreme refractive indices: hematite and rutile, *Astron. Astrophys.*, 446, 525–535, 2006.
- Nickovic, S., Vukovic, A., Vujadinovic, M., Djurdjevic, V., and Pejanovic, G.: Technical Note: High-resolution mineralogical database of dust-productive soils for atmospheric dust modeling, *Atmos. Chem. Phys.*, 12, 845–855, doi:10.5194/acp-12-845-2012, 2012.
- Nickovic, S., Vukovic, A., and Vujadinovic, M.: Atmospheric processing of iron carried by mineral dust, *Atmos. Chem. Phys.*, 13, 9169–9181, doi:10.5194/acp-13-9169-2013, 2013.
- Onari, S., Arai, T., and Kudo, K.: Infrared lattice vibrations and dielectric dispersion in α -Fe₂O₃, *Phys. Rev. B*, 16, 1717–1721, 1977.
- Osborne, S. R., Johnson, B. T., Haywood, J. M., Baran, A. J., Harrison M. A. J., and McConnell, C. L.: Physical and optical properties of mineral dust aerosol during the Dust and Biomass-burning Experiment, *J. Geophys. Res.-Atmos.*, 113, D00C03, doi:10.1029/2007JD009551, 2008.
- Otto, S., Bierwirth, E., Weinzierl, B., Kandler, K., Esselborn, M., Tesche, M., Schladitz, A., Wendisch, M., and Trautmann, T.: Solar radiative effects of a Saharan dust plume observed during SAMUM assuming spheroidal model particles, *Tellus B*, 61, 270–296, 2009.
- Painter, T. H., Deems, J. S., Belnap, J., Hamlet, A. F., Landry, C. C., and Udall, B.: Response of Colorado River runoff to dust radiative forcing in snow, *P. Natl. Acad. Sci. USA*, 107, 17125–17130, 2010.
- Patterson, E. and Gillette, D.: Commonalities in measured size distributions for aerosols having a soil-derived component, *J. Geophys. Res.*, 82, 2074–2082, 1977.
- Peterson, J. T.: Measurement of Atmospheric Aerosols and Infrared Radiation over Northwest India and their Relationship, PhD thesis, Dep. of Meteorol., Univ. of Wis., Madison, 1968.
- Petzold, A., Rasp, K., Weinzierl, B., Esselborn, M., Hamburger, T., Dörnbrack, A., Kandler, K., Schütz, L., Knippertz, P., and Fiebig, M.: Saharan dust absorption and refractive index from aircraft-based observations during SAMUM 2006, *Tellus B*, 61, 118–130, 2009.
- Petzold, A., Veira, A., Mund, S., Esselborn, M., Kiemle, C., Weinzierl, B., Hamburger, T., Ehret, G., Lieke, K., and Kandler, K.: Mixing of mineral dust with urban pollution aerosol over Dakar (Senegal): impact on dust physico-chemical and radiative properties, *Tellus B*, 63, 619–634, 2011.
- Popova, S., Tolstykh, T., and Ivlev, L.: Optical-Constants of Fe₂O₃ in infrared spectral region, *Optika Spektrosc.*, 35, 954–955, 1973.
- Postma, D. and Brockenhuus-Schack, B. S.: Diagenesis of iron in proglacial sand deposits of late- and post-Weichselian age, *J. Sediment. Res.*, 57, 1040–1053, 1987.
- Poulton, S. W. and Canfield, D. E.: Development of a sequential extraction procedure for iron: implications for iron partitioning in continentally derived particulates, *Chem. Geol.*, 214, 209–221, 2005.
- Qin, Y. and Mitchell, R. M.: Characterisation of episodic aerosol types over the Australian continent, *Atmos. Chem. Phys.*, 9, 1943–1956, doi:10.5194/acp-9-1943-2009, 2009.
- Querry, M. R.: Optical Constants, Contractor report, US Army Chemical Research, Development and Engineering Center (CRDC), Aberdeen Proving Ground, MD, 418 pp., 1985.
- Querry, M. R.: Optical Constants of Minerals and Other Materials from the Millimeter to the Ultraviolet, CRDEC-CR88009, US Army Chemical Research, Development and Engineering Center, Aberdeen Proving Ground, MD, 331 pp., 1987.
- Querry, M. R., Osborne, G., Lies, K., Jordon, R., and Coveney Jr., R. M.: Complex refractive index of limestone in the visible and infrared, *Appl. Optics*, 17, 353–356, 1978.
- Raiswell, R. and Anderson, T.: Reactive Iron Enrichment in Sediments Deposited Beneath Euxinic Bottom Waters: Constraints on Supply by Shelf Recycling, Special Publications, Geological Society, London, 248, 179–194, 2005.
- Redmond, H. E., Dial, K. D., and Thompson, J. E.: Light scattering and absorption by wind blown dust: theory, measurement, and recent data, *Aeolian Res.*, 2, 5–26, 2010.
- Reynolds, R. L., Goldstein, H. L., Moskowitz, B. M., Bryant, A. C., Skiles, S. M., Kokaly, R. F., Flagg, C. B., Yauk, K., Berquó, T.,

- and Breit, G.: Composition of dust deposited to snow cover in the Wasatch Range (Utah, USA): controls on radiative properties of snow cover and comparison to some dust-source sediments, *Aeolian Res.*, 15, 73–90, 2013.
- Reynolds, R. L., Cattle, S. R., Moskowicz, B. M., Goldstein, H. L., Yauk, K., Flagg, C. B., Berquó, T. S., Kokaly, R. F., Morman, S., and Breit, G. N.: Iron oxide minerals in dust of the Red Dawn event in eastern Australia, September 2009, *Aeolian Res.*, 15, 1–13, 2014.
- Ryder, C. L., Highwood, E. J., Rosenberg, P. D., Trembath, J., Brooke, J. K., Bart, M., Dean, A., Crosier, J., Dorsey, J., Brindley, H., Banks, J., Marsham, J. H., McQuaid, J. B., Sodemann, H., and Washington, R.: Optical properties of Saharan dust aerosol and contribution from the coarse mode as measured during the Fennec 2011 aircraft campaign, *Atmos. Chem. Phys.*, 13, 303–325, doi:10.5194/acp-13-303-2013, 2013.
- Scanza, R. A., Mahowald, N., Ghan, S., Zender, C. S., Kok, J. F., Liu, X., Zhang, Y., and Albani, S.: Modeling dust as component minerals in the Community Atmosphere Model: development of framework and impact on radiative forcing, *Atmos. Chem. Phys.*, 15, 537–561, doi:10.5194/acp-15-537-2015, 2015.
- Scheinost, A., Chavernas, A., Barrón, V., and Torrent, J.: Use and limitations of second-derivative diffuse reflectance spectroscopy in the visible to near-infrared range to identify and quantify Fe oxide minerals in soils, *Clay Clay Miner.*, 46, 528–536, 1998.
- Scheuvs, D., Kandler, K., Küpper, M., Lieke, K., Zorn, S., Ebert, M., Schütz, L., and Weinbruch, S.: Individual-analysis of airborne dust samples collected over Morocco in 2006 during SAMUM 1, *Tellus B*, 63, 512–530, 2011.
- Schladitz, A., Müller, T., Kaaden, N., Massling, A., Kandler, K., Ebert, M., Weinbruch, S., Deutscher, C., and Wiedensohler, A.: In situ measurements of optical properties at Tinfou (Morocco) during the Saharan mineral dust experiment SAMUM 2006, *Tellus B*, 61, 64–78, 2009.
- Schroth, A. W., Crusius, J., Sholkovitz, E. R., and Bostick, B. C.: Iron solubility driven by speciation in dust sources to the ocean, *Nat. Geosci.*, 2, 337–340, 2009.
- Schwertmann, U.: Relations between iron oxides, soil color, and soil formation, in: *Soil Science Society of America*, edited by: Bigham, J. M. and Ciolkosz, E. J., *Soil Color*, Special Pub., Madison, WI, Vol. 31., 51–69, 1993.
- Shao, Y., Wyrwoll, K.-H., Chappell, A., Huang, J., Lin, Z., McTainsh, G. H., Mikami, M., Tanaka, T. Y., Wang, X., and Yoon, S.: Dust cycle: an emerging core theme in Earth system science, *Aeolian Res.*, 2, 181–204, 2011.
- Shen, Z., Cao, J., Zhang, X., Arimoto, R., Ji, J., Balsam, W., Wang, Y., Zhang, R., and Li, X.: Spectroscopic analysis of iron-oxide minerals in aerosol particles from northern China, *Sci. Total Environ.*, 367, 899–907, 2006.
- Shettle, E. P. and Fenn, R. W.: Models for the Aerosols of the Lower atmosphere and the Effects of Humidity Variations on their Optical Properties, Environmental Research Papers, No. 676, AFGL-TR-79-0214, USAF, 94 pp., 1979.
- Shi, Z., Shao, L., Jones, T., and Lu, S.: Microscopy and mineralogy of airborne particles collected during severe dust storm episodes in Beijing, China, *J. Geophys. Res.-Atmos.*, 110, D01303, doi:10.1029/2004JD005073, 2005.
- Shi, Z., Krom, M. D., Bonneville, S., Baker, A. R., Jickells, T. D., and Benning, L. G.: Formation of iron nanoparticles and increase in iron reactivity in mineral dust during simulated cloud processing, *Environ. Sci. Technol.*, 43, 6592–6596, 2009.
- Shi, Z., Bonneville, S., Krom, M. D., Carslaw, K. S., Jickells, T. D., Baker, A. R., and Benning, L. G.: Iron dissolution kinetics of mineral dust at low pH during simulated atmospheric processing, *Atmos. Chem. Phys.*, 11, 995–1007, doi:10.5194/acp-11-995-2011, 2011.
- Shi, Z., Krom, M. D., Jickells, T. D., Bonneville, S., Carslaw, K. S., Mihalopoulos, N., Baker, A. R., and Benning, L. G.: Impacts on iron solubility in the mineral dust by processes in the source region and the atmosphere: a review, *Aeolian Res.*, 5, 21–42, 2012.
- Smith, A. J. and Grainger, R. G.: Does variation in mineral composition alter the short-wave light scattering properties of desert dust aerosol?, *J. Quant. Spectrosc. Ra.*, 133, 235–243, 2014.
- Sokolik, I. N., Winker, D., Bergametti, G., Gillette, D., Carmichael, G., Kaufman, Y., Gomes, L., Schuetz, L., and Penner, J.: Introduction to special section: outstanding problems in quantifying the radiative impacts of mineral dust, *J. Geophys. Res.-Atmos.*, 106, 18015–18027, 2001.
- Sokolik, I. N. and Toon, O. B.: Incorporation of mineralogical composition into models of the radiative properties of mineral aerosol from UV to IR wavelengths, *J. Geophys. Res.-Atmos.*, 104, 9423–9444, 1999.
- Song, X. and Boily, J.-F.: Carbon dioxide binding at dry FeOOH mineral surfaces: evidence for structure-controlled speciation, *Environ. Sci. Technol.*, 47, 9241–9248, 2013.
- Steyer, T. R.: Infrared optical properties of some solids of possible interest in astronomy and atmospheric physics, PhD thesis, Dep. of Phys., Univ. of Ariz., Tucson, 1974.
- Sumner, M.: Effect of iron oxides on positive and negative charges in clays and soils, *Clay Miner. Bull.*, 5, 218–226, 1963.
- Takahashi, Y., Higashi, M., Furukawa, T., and Mitsunobu, S.: Change of iron species and iron solubility in Asian dust during the long-range transport from western China to Japan, *Atmos. Chem. Phys.*, 11, 11237–11252, doi:10.5194/acp-11-11237-2011, 2011.
- Takahashi, Y., Furukawa, T., Kanai, Y., Uematsu, M., Zheng, G., and Marcus, M. A.: Seasonal changes in Fe species and soluble Fe concentration in the atmosphere in the Northwest Pacific region based on the analysis of aerosols collected in Tsukuba, Japan, *Atmos. Chem. Phys.*, 13, 7695–7710, doi:10.5194/acp-13-7695-2013, 2013.
- Tegen, I., Hollrig, P., Chin, M., Fung, I., Jacob, D., and Penner, J.: Contribution of different aerosol species to the global aerosol extinction optical thickness: estimates from model results, *J. Geophys. Res.-Atmos.*, 102, 23895–23915, 1997.
- Thomas, M. and Gautier, C.: Investigations of the March 2006 African dust storm using groundbased column-integrated high spectral resolution infrared (8–13 μm) and visible aerosol optical thickness measurements: 2. Mineral aerosol mixture analyses, *J. Geophys. Res.-Atmos.*, 114, D14209, doi:10.1029/2008JD010931, 2009.
- Tipping, E.: The adsorption of aquatic humic substances by iron oxides, *Geochim. Cosmochim. Ac.*, 45, 191–199, 1981.
- Torrent, J. and Barrón, V.: Diffuse reflectance spectroscopy of iron oxides, in: *Encyclopedia of Surface and Colloid Science*, Marcel Dekker, Inc., New York, 1438–1446, 2002.
- Wagner, R., Ajtai, T., Kandler, K., Lieke, K., Linke, C., Müller, T., Schnaiter, M., and Vragel, M.: Complex refractive in-

- dices of Saharan dust samples at visible and near UV wavelengths: a laboratory study, *Atmos. Chem. Phys.*, 12, 2491–2512, doi:10.5194/acp-12-2491-2012, 2012.
- Wijenayaka, L. A., Rubasinghege, G., Baltrusaitis, J., and Grassian, V. H.: Surface chemistry of α -FeOOH nanorods and microrods with gas-phase nitric acid and water vapor: insights into the role of particle size, surface structure, and surface hydroxyl groups in the adsorption and reactivity of α -FeOOH with atmospheric gases, *J. Phys. Chem. C*, 116, 12566–12577, 2012.
- Yang, S., Sheng, Y., Han, Y., and Chen, S.: Diffuse reflectance spectroscopic analysis of iron-oxide minerals in dust aerosol from Golmud, *J. Lanzhou University (Natural Sciences)*, 50, 710–715, 2014.
- Zhang, X., Gong, S., Shen, Z., Mei, F., Xi, X., Liu, L., Zhou, Z., Wang, D., Wang, Y., and Cheng, Y.: Characterization of soil dust aerosol in China and its transport and distribution during 2001 ACE-Asia: 1. Network observations, *J. Geophys. Res.-Atmos.*, 108, 4261, doi:10.1029/2002JD002632, 2003.
- Zhu, A., Ramanathan, V., Li, F., and Kim D.: Dust plumes over the Pacific, Indian, and Atlantic oceans: Climatology and radiative impact, *J. Geophys. Res.-Atmos.*, 112, D16208, doi:10.1029/2007JD008427, 2007.